A myeloid program associated with COVID-19 severity is decreased by therapeutic blockade of IL-6 signaling

Jason A. Hackney[#1], Haridha Shivram[#1], Jason Vander Heiden[1], Chris Overall[1], Luz Orozco[1], Xia Gao[1], Nathan West, Aditi Qamra[2], Diana Chang[1], Arindam Chakrabarti[1], David F. Choy[1], Alexis J. Combes[3], Tristan Courau[3], Gabriela K. Fragiadakis[3], Arjun Arkal Rao[3], Arja Ray[3], Jessica Tsui[3], Kenneth Hu[3], Nicholas F. Kuhn[3], Matthew F. Krummel[3], David J. Erle[3], Kirsten Kangelaris[3], Aartik Sarma[3], Zoe Lyon[3], Carolyn S. Calfee[3], Prescott G. Woodruff[3], Rajani Ghale[3], Eran Mick[3], Ashley Byrne[3], Beth Shoshana Zha[3], Charles Langelier[3], Carolyn M. Hendrickson[3], Monique G.P. van der Wijst[4], George C. Hartoularos[3], Tianna Grant[3], Raymund Bueno[3], David S. Lee[3], John R. Greenland[3], Yang Sun[3], Richard Perez[3], Anton Ogorodnikov[3], Alyssa Ward[3], Chun Jimmie Ye[3], UCSF COMET Consortium[3], Thiru Ramalingam[1], Jacqueline M. McBride[1], Fang Cai[1], Anastasia Teterina[2], Min Bao[1], Larry Tsai[1], Ivan O. Rosas[5], Aviv Regev[1], Sharookh B. Kapadia[1], Rebecca N. Bauer[1], Carrie M. Rosenberger[1*]

1. Genentech, Inc. 1 DNA Way, South San Francisco, CA 94080, USA.
2. Hoffman-La Roche Limited. 7070 Mississauga Road. Mississauga, ON L5N 5M8 Canada
3. University of California San Francisco, San Francisco, CA, USA.
4. Department of Genetics, University of Groningen, University Medical Center Groningen, Groningen, The Netherlands.
5. Baylor College of Medicine, 7200 Cambridge St, Houston, TX 77030, USA
[#]J.A. Hackney and H. Shivram are co-first authors.

*Corresponding author: Carrie M Rosenberger, Rosenberger.carrie@gene.com , 1-650-467-9065

Additional UCSF COMET Consortium authors are listed in the acknowledgements

Word count: 10 526, abstract: 200 words
Tables/Figures: 7 Figures, 1 Table, 7 supplemental Figures, 1 supplemental Table

Conflict of Interest Statement

J.A.H., H.S., J.V.H., C.O., L.O., X.G., N.W., A.Q., D.C., A.C, D.F.C., T.R, J.M.M., F.C., A.T., M.B., L.T., A.R., S.B.K., R.N.B., and C.M.R. were employees of Genentech, Inc. at the time of this study and own equity in Roche. The COMET study was supported in part by Genentech funding. C.J.Y. is a Scientific Advisory Board member for and holds equity in Related Sciences and ImmunAI, a consultant for and holds equity in Maze Therapeutics, and a consultant for TReX Bio. C.J.Y. has received research support from Chan Zuckerberg Initiative, Chan Zuckerberg Biohub, and Genentech. C.S.C. has received research funding from Roche-Genentech for an unrelated project as well as from NIH, DOD, and Quantum Leap Healthcare Collaborative. C.S.C. is a consultant for Vasomune, Quark, and Gen1e Life Sciences. C.H. is a consultant for Spring Discovery but does not have any financial interest in the company nor is the work related to what is covered in this manuscript. AR is a co-founder and equity holder of Celsius Therapeutics, an equity holder in Immunitas Therapeutics and, until 31 July 2020, was a scientific advisory board member of ThermoFisher Scientific, Syros Pharmaceuticals, Asimov and Neogene Therapeutics. AR is a named inventor on multiple patents related to single cell and spatial genomics filed by or issued to the Broad Institute.

Summary

Altered myeloid inflammation and lymphopenia are hallmarks of severe infections, including SARS-CoV-2. Here, we identified a gene program, defined by correlation with EN-RAGE (*S100A12*) gene expression, which was up-regulated in patient airway and blood myeloid cells. The EN-RAGE program was expressed in 7 cohorts and observed in patients with both COVID-19 and acute respiratory distress syndrome (ARDS) from other causes. This program was associated with greater clinical severity and predicted future mechanical ventilation and death. EN-RAGE^{+} myeloid cells express features consistent with suppressor cell functionality, with low HLA-DR and high PD-L1 surface expression and higher expression of T cell-suppressive genes. Sustained EN-RAGE signature expression in airway and blood myeloid cells correlated with clinical severity and increasing expression of T cell dysfunction markers, such as PD-1. IL-6 upregulated many of the severity-associated genes in the EN-RAGE gene program *in vitro*, along with potential mediators of T cell suppression, such as IL-10. Blockade of IL-6 signaling by tocilizumab in a placebo-controlled clinical trial led to rapid normalization of ENRAGE and T cell gene expression. This identifies IL-6 as a key driver of myeloid dysregulation associated with worse clinical outcomes in COVID-19 patients and provides insights into shared pathophysiological mechanisms in non-COVID-19 ARDS.

Keywords

Acute respiratory distress syndrome; COVID-19; myeloid; inflammation; lung injury; myeloid-derived suppressor cells; IL-6; reverse translation; infectious disease; monocyte; neutrophil

Introduction

Altered myeloid cell expression states, including the accumulation of cells with hallmarks of myeloid-derived suppressor cells (MDSC), are consistent features in the blood of COVID-19 patients, and serve as a hallmark of severity (1–18). Monocytes and granulocytes associated with increased COVID-19 severity exhibit low expression of HLA-DR, and high expression of hallmark MDSC genes such as *S100A12* (EN-RAGE), and can impair T cell activation via contact-dependent (i.e., PD-L1) and soluble mechanisms, including IL-10, TGF-β, arginase 1, IDO-dependent tryptophan metabolism, and reactive oxygen and nitrogen species (reviewed in (19–22)). Presence of MDSCs in severe COVID-19 patients, and patients with other severe infections, correlates with reduced T cell numbers, and can impair T cell proliferation and IFN-γ production *ex vivo* (23–28). Reduced T cell proliferation and tissue sequestration can in turn contribute to the lymphopenia observed in COVID-19 patients with severe disease, which increases with the severity of respiratory failure and is prognostic for higher mortality(29). Thus, understanding the role of myeloid suppressor cells and the pathways leading to their dysregulation is of critical importance in COVID-19 and other infections.

The pathways driving myeloid inflammation and the mechanistic connection of maladaptive cellular programs to severe disease and response to drug interventions are not yet understood. IL-6 is a key regulator of inflammation and has been proposed as a potential driver of dysfunctional myeloid immune response in cancer, COVID-19, and other diseases (10, 12, 20, 26, 30–33). IL-6 treatment *in vitro* leads to differentiation of hematopoietic stem cells into $CD14^+$ monocytes expressing a similar expression program to that observed in COVID-19 patient monocytes, including high expression of EN-RAGE and low expression of HLA-DR(10). Circulating IL-6

92 levels positively correlate with this severity-associated myeloid state in COVID-19 and other
93 severe infections(10). It has been suggested that treatment with IL-6-blocking antibodies
94 normalizes alterations in the myeloid compartment that are associated with disease severity(12), a
95 hypothesis requiring placebo-controlled trials to test. Samples from hospitalized COVID-19
96 patients treated with tocilizumab (a monoclonal antibody against IL6R/Actemra) in a placebo-
97 controlled study (COVACTA, n=438 hospitalized COVID-19 patients with hypoxemia
98 randomized 2:1 tocilizumab:placebo) provided a unique opportunity to evaluate the role of IL-6 in
99 shaping myeloid inflammation in patients(34). A meta-analysis by the World Health Organization
100 concluded that IL-6 antagonists reduce 28-day mortality in patients hospitalized for COVID-
101 19(35).
102
103 Here, we used single cell RNA-seq (scRNA-seq) of peripheral blood mononuclear cells (PBMCs)
104 and bronchoalveolar lavage (BAL) fluid cells collected from COVID-19 patients, to identify a
105 myeloid cell program shared across tissue compartments, defined by high expression of the EN-
106 RAGE gene, among other inflammatory markers. Expression of this program was associated with
107 more severe disease in our discovery cohorts. We replicated this finding using data from the
108 COMET observational study, which includes sampling from endotracheal aspirates (ETA), whole
109 blood, and PBMCs (2, 36, 37) of COVID-19 patients. Combined single cell profiling of RNA and
110 cell surface proteins (CITE-seq) characterized the immunosuppressive expression program in EN-
111 RAGE signature expressing cells and connected it to cell surface phenotypes of impaired myeloid
112 antigen presentation and T cell dysfunction. The EN-RAGE expression program was associated
113 with several measures of COVID-19 clinical severity and outcomes and was also observed in
114 patients with acute respiratory distress syndrome (ARDS) from other causes, identifying a

115 targetable pathway relevant to ARDS. Finally, blocking IL-6 signaling using tocilizumab in an
116 interventional setting reduced expression of the EN-RAGE signature and normalized T cell
117 numbers in COVID-19 patients from the COVACTA trial, providing mechanistic insight into the
118 therapeutic response to COVID-19 patients to IL-6 blockade.
119

120 **Results**

121 ***A pan-myeloid EN-RAGE signature in blood and airway samples is associated with severe***
122 ***COVID-19***

123 We used publicly available scRNA-seq data from COVID-19 patients to define a gene program
124 that classifies a shared myeloid state across airway and blood samples. We seeded the program by
125 the expression of the gene encoding EN-RAGE (*S100A12*), which has been implicated in several
126 myeloid populations in the peripheral blood associated with COVID-19 severity(2, 10, 38, 39).
127 EN-RAGE expression is upregulated by IL-6(40), is elevated in the airways of ARDS patients as
128 well as other lung diseases(41), and serum levels correlate with COVID-19 severity(1, 4). We
129 identified a set of 84 genes that co-vary (Pearson's $r > 0.5$) with EN-RAGE expression across
130 myeloid cells from bronchoalveolar lavage (BAL) fluid and PBMCs from COVID-19 patients(7,
131 11) (**Figure. 1A**; **Table S1**). This gene program showed strong coordinated expression across
132 airway and blood samples and predominant expression in many myeloid cell types (monocytes,
133 neutrophils, and macrophages), although dendritic cells (DCs) and non-classical monocytes
134 showed lower overall expression (**Figure. S1**). Increased expression of the EN-RAGE program in
135 neutrophil, monocyte and macrophage subsets was associated with greater clinical severity in both
136 blood and airway samples (**Figure. 1B** and **Figure. S1C**).
137

138 The EN-RAGE program scores correlated with the scores of a previously-defined MS1 gene set
139 (9), which was associated with increased severity in COVID-19 and sepsis patients(9, 10)
140 (Spearman's ρ=0.64 and 0.95 in pseudobulk expression profiles of blood and airway monocytes
141 and neutrophils (5 cohorts) and ρ=0.65 in whole lung myeloid cells (one cohort) (all $p<0.0001$)).
142 Only seven genes (CLU, CYP1B1, LILRA5, NAMPT, S100A12, S100A8, VCAN) are shared
143 between the 84 genes in the EN-RAGE program and the 23 genes in the MS1 signature identified
144 in COVID-19 patients(10), which is a significant overlap (p-value=7e-14, hypergeometric test).
145 EN-RAGE program expression was more highly intercorrelated than the MS1 signature across
146 sample types (**Figure. S2A)**. While MS1 had strong pairwise correlations in PBMC myeloid cells,
147 many genes were no longer correlated when measured in whole blood (WB) or endotracheal
148 aspirate (ETA) (**Figure. S2B-M)**. Because of the reduced performance of MS1 outside of PBMCs,
149 we used the EN-RAGE program (denoted EN-RAGE$^+$) in subsequent analyses to more specifically
150 evaluate myeloid cells in bulk RNA-seq from whole blood and airway samples, which have greater
151 cellular complexity than PBMC samples.
152

153 ***EN-RAGE signature is associated with acute lung injury from diverse causes***

154 We next hypothesized that the EN-RAGE myeloid program may also be a feature of non-COVID-
155 19 lung injury. To test this hypothesis, we scored the EN-RAGE program in samples from the
156 COMET observational cohort, where 75 patients with either COVID-19 or acute lung injury from
157 other causes were followed longitudinally (**Table 1**, patient characteristics)(2, 36, 37). Whole
158 blood (WB), PBMC, and endotracheal aspirates (ETA) were sampled and profiled by scRNA-Seq.
159 This cohort offers rich clinical and molecular phenotyping to allow single-cell dissection of the
160 connection between the airways and the blood at the mRNA and protein level, and how this relates

161 to clinical outcomes. EN-RAGE signature expression was highest in monocytes, macrophages,
162 and neutrophils, consistent with our previous analyses (**Figure 2** and **Figure S2**). EN-RAGE$^+$
163 myeloid cells were present in the blood and airways in both COVID-19 and non-COVID-19 acute
164 lung injury patients, highlighting the generality of this program (**Figure 2C**).
165

166 ***EN-RAGE signature expression correlates with clinical severity and is prognostic for worse***
167 ***clinical outcomes***

168 In COVID-19 patients, EN-RAGE$^+$ myeloid cells were associated with increased clinical severity
169 at presentation, as defined by the extent of respiratory support required at study enrollment, in
170 monocytes (PBMC, **Figure 2C** and **Figure S1C**) and neutrophils (whole blood, **Figure 2C**). The
171 severity association of monocyte ENRAGE score observed in PBMC was not observed in the
172 smaller number of samples available from whole blood. An association with severity is not found
173 in ETA samples, perhaps since this sample type is only obtained from critically ill patients on
174 mechanical ventilation and so a milder severity group is lacking.
175

176 We next asked whether higher EN-RAGE signature expression predicts worse patient outcomes.
177 In PBMC samples from COVID-19 and non-COVID-19 patients at COMET study enrollment, the
178 EN-RAGE program score was associated not only with greater baseline clinical severity (NIH
179 COVID-19 severity ordinal score) but also worse clinical outcomes (ICU admission $p<0.01$and
180 maximal NIH ordinal scale: Spearman $\rho=0.30$ $p=0.02$) (**Figure 3A** and **Figure S3A-C**). However,
181 these associations were no longer significant once baseline severity measures were considered in
182 our analyses ($p>0.5$, data not shown), possibly because of the limited numbers of patients in this
183 cohort and the increased risk of severe outcomes in patients presenting with greater severity. EN-

184 RAGE program expression was not significantly associated with age (Spearman ρ=-0.02, p=0.88)
185 nor with days from symptom onset to study enrollment (Spearman ρ=0.09, p=0.57). EN-RAGE
186 score was higher in patients who presented with or later developed ARDS compared with those
187 who did not by either AECC or Berlin diagnostic criteria ($p<0.01$ for AECC definition, $p<0.05$ for
188 Berlin definition) (**Figure S3D-E**). ENRAGE score was higher in ARDS (AECC definition)
189 resulting from SARS-CoV-2 infection or other etiology ($p<0.05$) (**Figure 3B**), but the difference
190 in the smaller patient subgroups was not significant when using the more stringent Berlin ARDS
191 definition (**Figure S3F**).
192

193 Leveraging the availability of longitudinal samples from ventilated patients in the COMET cohort,
194 there was a significant association between the temporal trajectory of airway EN-RAGE
195 expression in each patient and patient outcomes (**Figure 3C).** To test this, we stratified patients
196 into two groups by the number of ventilator-free days (VFD) and compared the slope of the
197 regression lines of the two groups. Airway EN-RAGE expression decreased over time in survivors
198 with fewest days of ventilation and increased in patients who died or had ≥28 days of ventilation
199 ($p<0.05$ linear mixed model, ETA, **Figure 3C**). Worse clinical outcomes are accompanied by
200 sustained elevated airway levels of EN-RAGE$^+$ cells as well as higher baseline levels in the blood.
201

202 ***EN-RAGE program expression in myeloid cells is associated with increased markers of***
203 ***immunosuppression in blood and airways***
204 The EN-RAGE program score was also associated with expression of genes characteristic of
205 MDSCs, suggesting one path through which EN-RAGE$^+$ cells may contribute to clinical severity.
206 Specifically, EN-RAGE program expression was correlated with metrics of suppressed myeloid

207 and lymphoid states across another five COVID-19 cohorts(2, 5, 7, 11, 12, 36, 37), spanning ETA,
208 BAL, lung, PBMC, and blood samples (complete results in **Table S2**). For example, in COMET
209 PBMC monocytes, EN-RAGE program expression correlated with high *CD14* (Spearman ρ=0.65,
210 $p<0.001$), *CCR2* (ρ=0.25, $p<0.05$) and *PTGER2* (ρ=0.38, $p<0.001$) (**Figure 3D**). *CCR2* and
211 *PTGER2* are two receptors important for myeloid cell recruitment to the infected lung via *CCL2*
212 and prostaglandins, respectively. EN-RAGE program expression correlated with low expression
213 of MHC class II genes, suggesting reduced capacity for antigen presentation (*HLADRA:* ρ=-0.45
214 and *HLADRB1:* ρ=-0.48, $p<0.001$, **Figure 3D** and **Table S2**). In blood monocytes, there was a
215 positive correlation with *STAT3*, a key transcription factor regulating MDSC gene expression
216 (ρ=0.79, $p<0.001$, **Figure 3D**). MDSCs can suppress T cells using context-specific mechanisms
217 across sites of infection or malignancy, and the mechanisms used can also differ depending on
218 whether they originate from the monocytic or granulocytic lineage(13, 20). In blood monocytes,
219 EN-RAGE program expression was positively correlated with expression of genes encoding
220 effectors that can suppress T cells through reactive oxygen species (*CYBB/PHOX*) and
221 prostaglandins (*PTGER2*), and *TGFβ1*, but inconsistent associations with arginase (*ARG1*) and
222 tryptophan depletion (*IDO1*) across cohorts (**Figure 3D** and **Table S2**). Granulocytic EN-RAGE$^+$
223 cells had similar associations as their monocytic counterparts, with notable differences including
224 stronger correlations with *PDL1* and *TGFβ1* and little to no association with reactive oxygen
225 species (*CYBB/PHOX*) and *PTGER2* compared with EN-RAGE$^+$ monocytes (**Figure 3D** and
226 **Table S2**). Consistent with MDSCs characterized in other infections and cancers(20, 22, 42), EN-
227 RAGE$^+$ cells expressed higher levels of multiple potential mediators of immunosuppression
228 (*PDL1*, *CYBB/PHOX*, and *TGFβ1*) with some genes preferentially expressed by monocytic
229 lineages (i.e. *CYBB/PHOX* ρ>0.4, **Table S2**) or granulocytic lineages (i.e. *TGFβ1* ρ>0.6, **Table**

230 **S2**) (**Table S2**). EN-RAGE program expression in PBMC myeloid cells was modestly correlated
231 with plasma protein levels of IL-6, a potential driver of MDSCs, and IL-10, a potential mediator
232 of T cell suppression (Spearman ρ=0.41, p=0.005 and ρ=0.29, p=0.05, respectively; **Figure 3E**).
233

234 These associations were also largely observed in airways samples, suggesting an overall consistent
235 phenotype in both the blood and the infected lung (**Figure 3D**). As in the blood, EN-RAGE
236 program expression in monocytes and neutrophils was positively correlated with*, STAT3* in ETA
237 samples but lacked the correlations with *CCR2* and *HLADR*, showed stronger correlations with
238 *CCR5*, and inconsistent relationships with *CYBB* and *CD14* (**Figure 3D** and **Table S2**). EN-
239 RAGE^{+} monocytes and neutrophils cells in lung and airway samples (ETA, BAL, and lung post-
240 mortem autopsy tissue) had increased association with *PDL1*, *IL10, TGFβ, IDO,* and *IL1β*, which
241 can suppress T cell function, compared to the blood (**Figure 3D,F** and **Table S2**). Peripheral blood
242 myeloid cells expressed lower levels of *IL10* and *IL1β* and had weaker correlation with the EN-
243 RAGE signature when transcripts were detected, illustrating the importance of sampling infected
244 tissues and establishing blood correlates of tissue immune responses (**Figure 3D** and **Table S2**).
245 Across four patient cohorts, airway EN-RAGE^{+} monocytes and neutrophils consistently expressed
246 multiple markers of inflammation with autoregulatory functions that can be immunosuppressive,
247 including *IL10, PDL1, TGFβ1, IL1β*, and *IDO* (**Table S2**).
248

249 **Characterization of EN-RAGE^{+} myeloid and T cell phenotypes**

250 To connect the EN-RAGE expression program to cellular phenotypes, we used CITE-seq data
251 from PBMCs in COMET to relate cell surface protein expression and EN-RAGE program
252 expression. The EN-RAGE signature was most highly expressed in CD14^{+}CD16^{lo}HLA-DR^{lo}

classical monocytes (cM) (**Figure 4A-B**), confirming the reduced antigen presentation capacity suggested by scRNA-seq data (**Table S2**). EN-RAGE signature scores on cMs positively correlated across patients with cM surface expression of 19 of the 188 CITE-Seq measured proteins (FDR<0.05, **Figure 4C**), including three markers characteristic of MDSCs: PD-L1 (CD274, Spearman ρ=0.43, FDR=0.008), podoplanin (PDPN, ρ=0.52, FDR=0.001), and CD38 (ρ=0.49, FDR=0.002), which is IL-6-inducible in tumors(43, 44). Conversely, EN-RAGE signature scores on cM were negatively correlated with 19 markers (FDR<0.05, **Figure 4C**), including HLA-DR (ρ=-0.73, FDR<0.0001), the T cell costimulatory protein CD40L (ρ=-0.36, FDR=0.03), the LFA subunit CD11A involved in trafficking and activation (ITGAL, ρ=-0.52, FDR=0.002), and two markers of granulocytic MDSCs (SIGLEC7: ρ=-0.52, FDR 0.001; CD244: ρ=-0.50, FDR=0.002) (**Figure 4C**).

EN-RAGE program scores in cMs also negatively correlated with the level of the activation marker CD40 on $CD4^+$ T cells (**Figure 4D**), consistent with the negative correlation of the expression of ligand CD40L on cMs with their EN-RAGE program (**Figure 4C**). Conversely, EN-RAGE program scores in cMs were positively correlated with two proteins expressed by exhausted $CD4^+$ and $CD8^+$ T cells: podoplanin/PDPN (Spearman ρ=0.37, FDR=0.04) and TNFSF14/LIGHT (ρ=0.39, p=0.03) (**Figure 4D-E**). These data support the EN-RAGE program activity in cMs correlating with distinct $CD8^+$ and $CD4^+$ T lymphocytes activation states across patients.

Moreover, the dynamic changes in EN-RAGE program expression and markers of myeloid activation and T cell dysfunction were associated with clinical outcomes. Patients with PBMC CITE-seq data were categorized into 4 outcome groups based on survival and the duration of

276 mechanical ventilation. In monocytes from patients with more severe outcomes compared with
277 patients not requiring ventilation, HLA-DR trended lower than healthy (indicated by red line) and
278 failed to recover to healthy levels over 14 days (**Figure 4F**), and trends of sustained higher PD-L1
279 and EN-RAGE score in some greater severity groups remained higher in ventilated patients
280 (**Figure 4G-H**). On $CD8^+$ and $CD4^+$ T cells, markers of T cell dysfunction or exhaustion (PD-1,
281 LAG3, TIGIT, CTLA4, and BTLA4) showed greater increases over 14 days in patients with
282 worsening outcomes (>7 days mechanical ventilation and/or death) compared with non-ventilated
283 patients (**Figure 4I-L** and **Figure S4**, Pearson correlation $p<0.05$, not significant for PD-1 on $CD4^+$
284 T cells). Therefore, the EN-RAGE myeloid expression program correlates with markers of a
285 suppressive cell surface phenotype on monocytes, and with reduced activation of $CD4^+$ and $CD8^+$
286 T cells, as indicated by increasing expression of T cell dysfunction markers over time (**Figure 4I-**
287 **L** and **Figure S4**).
288

289 ***IL-6 induces the EN-RAGE program in monocytes in vitro***

290 Several lines of evidence led us to hypothesize that IL-6 can be a regulator of the EN-RAGE
291 program. First, IL-6 treatment of HSPCs promotes upregulation of the MS1 gene signature in
292 monocytes(10), which correlates with the EN-RAGE program (Spearman $\rho \geq 0.64$ in monocytes,
293 $p<0.0001$ across 5 cohorts as described above). Moreover, blood monocyte EN-RAGE program
294 expression correlates with plasma IL-6 protein levels, and with levels of monocyte *STAT3* mRNA,
295 a transcription factor activated by IL-6 signaling (**Figure 3D-E** and **Table S2**). To test this
296 hypothesis, we treated human primary monocytes with IL-6 *in vitro* followed by RNA-seq.
297

298 IL-6 treatment altered the expression of 36 of 84 EN-RAGE program genes (Benjamini-Hochberg
299 FDR<0.05, **Figure 5A**), as well as of *IL10, IL1β, CYBB*, and *CCR2* (**Figure 5B**), all features of
300 EN-RAGE$^+$ monocytes in COVID-19 patients (**Figure 3D**). Using gene set enrichment analysis,
301 we found that IL-6 could partially up-regulate the expression of EN-RAGE and MS1 signature
302 genes (Benjamini-Hochberg adjusted p<0.001 and p<0.01, respectively; **Figure 5C**). Our data
303 suggest that IL-6 is sufficient to upregulate the expression of many ENRAGE program genes in
304 monocytes *in vitro*, including markers of a potentially T cell suppressive phenotype in patients.
305

306 ***The myeloid EN-RAGE program correlates with expression programs of suppressive myeloid***
307 ***cells and impaired T cells and with increased clinical severity in an interventional COVID-19***
308 ***clinical trial***

309 We next asked if blocking IL-6 signaling in patients correlated with a change in EN-RAGE
310 program expression, leveraging data from COVACTA, a double-blind randomized clinical trial of
311 tocilizumab (anti-IL6R/Actemra) in hospitalized COVID-19 patients with hypoxemia(34).
312 Consistent with our findings in other cohorts, bulk RNA-seq expression profiles from whole blood
313 collected at baseline from 438 patients showed higher normalized enrichment scores for the EN-
314 RAGE program in patients requiring positive pressure ventilation at baseline compared with those
315 who did not (**Figure 6A-B,** FGSEA Benjamini-Hochberg FDR < 0.05). The EN-RAGE gene set
316 was also enriched in patients needing future mechanical ventilation or progressing to death even
317 when controlling for the association with baseline severity (**Figure 6C-D**, FGSEA Benjamini-
318 Hochberg FDR<0.05). The prognostic relationship of the ENRAGE signature with mortality was
319 maintained even when adjusting for myeloid cell proportions in blood (**Figure S5A-E**; FDR<0.05,
320 FGSEA). Moreover, lower expression of gene sets classifying CD8$^+$ and CD4$^+$ T lymphocytes

321 (CIBERSORT(45)) was associated with worse clinical severity and outcomes (**Figure 6B-D**,
322 (Benjamini-Hochberg FDR<0.05). Furthermore, consistent with COMET whole blood scRNA-
323 seq, EN-RAGE program scores were positively correlated with expression of *PDL1, IL10,* and
324 *IL1β* in whole blood at day 1 in COVACTA patients (**Figure 7A**), as well as with serum protein
325 levels of EN-RAGE, IL-6, IL-10, IL-1β, and ARG1 (**Figure S7A**, t-test p<0.05). Examination of
326 T cell genes that were associated with EN-RAGE program expression in scRNA-seq data (**Figure**
327 **7A**) revealed that high myeloid EN-RAGE program expression in COVACTA bulk RNA-seq was
328 associated with low expression of T cell effectors (granzyme, perforin and lymphotoxin (*GZMB,*
329 *GZMM, PRF1, LTA*)), cytotoxicity (*FASL*), and *IFNG*), activation markers (*KLRK1/NKG2D*) and
330 dysfunction markers (*CTLA4, LAG3, CD160*). Many of these genes were expressed at a lower
331 level in patients with more severe disease (*IFNG*, *FASLG, CTLA4, LAG3, TIGIT, TBX21/Tbet,*
332 *XCL1*; **Figure 7B**, Benjamini-Hochberg FDR<0.05 and fold change < $\log_2$ -0.5). Higher EN-
333 RAGE program expression was also correlated with lower lymphocytes (ρ=-0.5) and monocytes
334 (ρ=-0.2) and increased neutrophils (ρ=0.5) (**Figure S7A**, all p<0.001). Thus, the COVACTA
335 cohort shows similar features to those observed in COMET, including the expression of the EN-
336 RAGE$^+$ myeloid program and its correlation with greater clinical severity and worse clinical
337 outcomes.
338

339 ***IL-6 blockade decreases the myeloid EN-RAGE state and increases T cells in COVID-19***
340 ***patients***

341 Finally, to understand the role of IL-6 in patients, we examined the effect of tocilizumab treatment
342 on the EN-RAGE myeloid state in COVID-19 patients and effect on T cells using longitudinal
343 samples from the COVACTA study(14, 34). Blockade of IL-6 signaling reduced expression of

344 many genes in the EN-RAGE program and increased T cell signature expression after 3 or 7 days
345 of tocilizumab treatment compared with placebo (**Figure 6A, E**; Benjamini-Hochberg FDR<0.05).
346 Consistent with the EN-RAGE program expression, MDSC and MS1 signatures were elevated in
347 patients with worse baseline clinical severity and needing future mechanical ventilation or who
348 died, and decreased following tocilizumab treatment (**Figure 6B-E**, Benjamini-Hochberg
349 FDR<0.05). These enrichments were consistently maintained when adjusted for blood cell type
350 composition (proportion of total leukocyte levels added as covariates to the DESeq2 model)
351 (**Figure S5A-C**). The effect of tocilizumab on gene set enrichment was comparable between
352 tertiles of baseline serum IL-6 protein levels (**Figure S5D-E**). EN-RAGE program gene expression
353 was sustained over the first 7 days in patients with worse clinical outcomes at day 28 (hospitalized
354 or non-survivor vs discharged, **Figure 6F**). The ENRAGE program was reduced following
355 tocilizumab treatment more than in placebo treatment over the first 7 days, particularly in patients
356 with better clinical outcomes (**Figure 6F** and **Figure S6A**). At the same time, CD8 T cell-
357 associated gene expression rapidly increased after tocilizumab treatment, again particularly in
358 patients that showed clinical improvement (**Figure 6F** and **Figure 7C**). Similar results were
359 observed for the MS1 severity-associated myeloid and CIBERSORT $CD4^+$ T cell gene sets
360 (**Figure S6B, D**). This corresponded with a more rapid increase in blood lymphocytes and decrease
361 in neutrophil cell counts in tocilizumab-treated patients who were discharged by 28 days compared
362 with placebo (**Figure S6E-J**). When we compared the change between day 7 and 1 in EN-RAGE
363 program expression with the change in measured blood cellularity, patients with a greater decrease
364 in EN-RAGE had a greater increase in blood lymphocytes and monocytes and decreases in
365 neutrophils (**Figure S7B-D**). This was more pronounced in patients treated with tocilizumab
366 compared with placebo.

The reduction in EN-RAGE program following IL-6 blockade corresponded with normalization of potential mediators and correlates of T cell suppression. Patients with a greater decrease in EN-RAGE program expression from day 1 to 7 had greater decreases in serum EN-RAGE, IL-10, IL-1β, and ARG1 protein levels, as indicated by a positive slope of the correlation line (**Figure S7E-H**). IL-6R blockade with tocilizumab resulted in a greater decrease in ENRAGE program expression, as indicated by a greater offset in the regression in the tocilizumab-treated arm compared with placebo, and a greater decrease in this set of serum proteins, as indicated by more green vs red dots in the bottom left quadrant (**Figure S7E-H**). This correlated with increased expression of the T cell genes *IFNG, FASLG, CTLA4* and *XCL1* in tocilizumab-treated patients (**Figure 7C**). In sum, blockade of IL-6 signaling in COVID-19 patients rapidly normalizes the severity-associated myeloid and T cell states, identified using both patient scRNA-seq data and the IL-6 *in vitro* model, to levels in healthy individuals, which correlates with clinical improvement by 28 days.

Discussion

While altered myeloid states are hallmarks of COVID-19 disease severity(1–18), the pathways driving maladaptive myeloid inflammation have not been clearly defined. This study supports a working model whereby IL-6 differentiates myeloid cells from both monocytic and granulocytic lineages to a suppressive phenotype characterized by low antigen presentation on HLA-DR and increased expression of multiple factors that can suppress T cells (IL-10, PD-L1, TGF-β1) (**Figure 7D**). We define a pan-myeloid ENRAGE program of coordinately-expressed genes in the airways and blood of COVID-19 patients that is prognostic for severe outcomes and

391 is robust across 7 cohorts(2, 5–7, 11, 12, 14, 36, 37). EN-RAGE$^+$ cells express multiple phenotypic
392 hallmarks of MDSCs by cell surface protein analysis: decreased capacity for antigen presentation
393 and co-stimulation through HLA-DR and CD40, and increased potential to suppress T cells
394 through PD-L1. This was associated with sustained elevated expression of markers on T cells
395 dysfunction such as PD-1 in patients with prolonged mechanical ventilation or who died. COVID-
396 19 patients with higher EN-RAGE signature expression had a greater risk of future mechanical
397 ventilation and mortality, and EN-RAGE$^+$ myeloid cell impairment of optimal T cell-mediated
398 immunity is one potential mechanism.

399 These data demonstrate the importance of IL-6 in altering immune cell phenotypes in
400 COVID-19 patients and provide a potential mechanism for the therapeutic benefit of tocilizumab
401 in patients hospitalized with COVID-19(35). Tocilizumab is approved for treating hospitalized
402 adult COVID-19 patients requiring supplemental oxygen and receiving corticosteroids by the US
403 Food and Drug Administration and the European Medicines Agency. IL-6 antagonists significantly
404 reduced mortality compared with usual care in a large meta-analysis using data from 27 trials(35).
405 While COVACTA did not meet the primary endpoint of improving clinical status on day 28,
406 tocilizumab demonstrated clinically meaningful benefits, such as shortening hospital stay by 8
407 days, compared with the placebo arm(34). Therapeutic blockade of IL-6 signaling with
408 tocilizumab attenuates expression of the EN-RAGE signature in blood cells and normalize T cell
409 numbers, correlating with clinical improvement. IL-6 alone does not significantly induce the entire
410 ENRAGE program, which is consistent with the partial IL-6R-dependent induction of the severity-
411 associated MS1 program by sepsis patient serum using an *in vitro* system(10). The effect of IL-6R
412 blockade in reducing the ENRAGE signature expression in patients was observed in survivors and

413 not non-survivors (**Figure 6F**), suggesting other potential factors besides IL-6 that regulate
414 expression of the full severity-associated transcriptional program.

415 COVID-19 patients with lymphopenia are at higher risk for worse clinical outcomes in the
416 COVACTA cohort(29). In addition to being reduced in numbers, suppressed T cell phenotypes
417 have been described in severe COVID-19 patients. Polyfunctional Th1 and Th17 $CD4^+$ and $CD8^+$
418 cell subsets are underrepresented in SARS-CoV-2 infection, with less proliferation and impaired
419 IFN-γ and IL-2 secretion following restimulation *in vitro*(46, 47). T cells with increased expression
420 of activation (OX40, CD69) and exhaustion (PD-1, TIGIT, TIM1) markers have been observed in
421 some(38, 48) but not all cohorts(49) and functional exhaustion of $CD8^+$ T cells has been
422 reported(50–52). In single cell analysis of the COMET cohort, a phenotype of sustained elevated
423 expression of PD-1, TIGIT, and LAG3 was observed on T cells in patients requiring longer
424 mechanical ventilation and non-survivors. As tocilizumab increased the number of circulating T
425 cells, the observed increase in markers of T cell function such as IFNγ and CD69 may result from
426 increased T cell abundance rather than increased functionality per cell. Differential regulation of
427 T cell genes suggests a potential effect of tocilizumab on T cell quality in addition to quantity. IL-
428 6R blockade increases markers of early polyfunctional T cells (*IFNG, XCL1, CD69*) and recently
429 activated/less exhausted cells (*IL7R*) while markers associated with broader spectrum of T cell
430 functional states (i.e. cytotoxic T cell markers T-bet (*TBX21*), perforin (*PRF1*), and granzymes
431 (*GZMM, GZMB*)) are less affected. However, there is limited ability to infer T cell functionality
432 from bulk RNA-seq data. Future studies using multi-dimensional flow cytometry data will enable
433 more precise definition of how IL-6 alters the T cell phenotype in COVID-19, both via myeloid
434 activation and acting directly on T cells. NK cells are important antiviral effector cells that can be
435 suppressed by MDSCs(19) and can express markers of dysfunction in COVID-19(49). A potential

436 connection between EN-RAGE+ myeloid cells and NK cells or the suppressive regulatory T cell
437 phenotype observed in severe COVID-19 patients(53) remains to be characterized.

438 Suppressive myeloid cells are one potential mechanism underlying impaired T cell
439 immunity in severe COVID-19. MDSCs express mediators of T cell suppression in a context-
440 dependent manner, depending on the type of infection or tumor(20, 22). MDSCs express multiple
441 genes through which they may potentially suppress T cells. Moreover, differential correlations
442 between the EN-RAGE signature and genes encoding immunosuppressive mediators were
443 observed between cell lineage (granulocytic vs. monocytic) and compartment (blood vs. airways).
444 MDSCs are often identified by low HLA-DR expression as a marker of impaired antigen
445 presentation capacity(23, 26–28, 46). Interestingly, while some features of EN-RAGE^{+} cells were
446 consistent between blood and airways (i.e. high PD-L1), the expression of other genes was tissue-
447 dependent, and the low expression of HLA-DR in the blood was lost in airway samples. This is
448 consistent with the observation that HLA-DR^{lo} MDSCs were not found in ETA airway samples by
449 flow cytometry(26). These data suggest that EN-RAGE^{+} myeloid cells home to the infected lung
450 and adopt a tissue-specific phenotype, with increasing expression of IL-10 and IDO and decreasing
451 expression of CCR2 and CYBB, highlighting the importance of characterizing immune responses
452 at the site of infection. The EN-RAGE^{+} myeloid state may underlie disease severity through
453 additional mechanisms. For example, EN-RAGE^{+} cells express higher *IL-1β* and *TGF-β1* which
454 can increase endothelial and epithelial cell permeability, respectively, and potential mechanisms
455 whereby EN-RAGE^{+} cells could affect barrier integrity and edema in patients with acute lung
456 injury remains to be explored(10, 54, 55).

457 This study connects immune cell phenotypes in the blood with the myeloid EN-RAGE
458 state in the airways using paired quantification of mRNA and surface proteins at single cell

459 resolution in PBMCs and ETA single cell transcriptomes from the COMET study and longitudinal
460 blood mRNA expression data from the large Phase 3 COVACTA study. The inclusion of patients
461 with acute lung injury from other causes in the COMET cohort reveals that EN-RAGE$^+$ myeloid
462 cells are relevant to insults in addition to SARS-CoV-2 infection, and identifies a targetable
463 pathway relevant to ARDS. IL-6 predicts severe patient outcomes(29) and has been hypothesized
464 to be a driver of myeloid differentiation in severe infections(10, 12). We show that tocilizumab
465 treatment rapidly normalized myeloid and T cell states to healthy control levels, which was
466 correlated with improved clinical outcomes. This study establishes the importance of IL-6 in
467 driving differentiation of the severity-associated EN-RAGE$^+$ myeloid state in patients. COVID-19
468 and cancer share risk factors, such as age and metabolic syndrome, and underlying
469 immunobiology, such as MDSCs and T cell dysfunction, making it appealing to speculate that EN-
470 RAGE$^+$ myeloid cells may contribute to pathology in multiple diseases.

Methods

Reanalysis of published scRNA-seq data

Raw count data from Schulte-Schrepping, *et al.*(11) were downloaded from http://fastgenomics.org. For analysis of the PBMC data collected using 10x Genomics droplet-based capture, and whole blood collected using Rhapsody microwell-based capture, the raw count data was reprocessed using scripts written in the R programming language(56) and packages from the Bioconductor project (https://www.bioconductor.org). Briefly, counts were normalized using the computeLibraryFactors method from the scater R package(57) and dimensionality reduction was performed using PCA followed by UMAP projection. For calculating PCA, the top 5000 most variable genes were selected, accounting for overall expression level using the modelGeneVar method from the scran R package(58). The UMAP projection was calculated using the first 10 principal components. Graph-based clustering was performed using the Louvain algorithm on the same 10 principal components. Marker genes for each cluster were determined using pairwise t-tests, calculated using the pairwiseTTest method from the scran R package, and were used to manually assign broad cell type labels to each cluster. Clusters from the same broad cell type classification were merged. The myeloid populations (monocytes, DCs and neutrophils) were separately re-clustered using the same procedures: the 5000 most variable genes were selected, used for PCA calculation, graph-based clustering and UMAP projection. Marker genes were calculated for each cluster, and clusters were manually assigned using the marker gene lists.

Raw sequencing reads from Liao, *et al.*(7) were downloaded from SRA (PRJNA608742). Sequencing data were then processed using cellranger v4.0.0 (10x Genomics, Pleasanton, CA, USA) using GRCh38 as the reference genome, and gene models from GENCODE (v27) for

494 assigning reads to genes. The emptyDrops method was used from the DropletUtils R package(59)
495 to identify barcodes that corresponded to cellular droplets. Any barcode with fewer than 200 UMIs
496 or 100 genes detected was removed. This allowed us to retain neutrophil-containing droplets, as
497 these are mostly removed by default processing using cellranger. Droplets with high abundance of
498 mitochondrial RNA (>10%) were removed. This yielded 90592 cells for further analysis. The same
499 procedures described above were used to normalize, cluster and annotate cells into broad
500 populations (macrophage, neutrophil, T cell, epithelial cell, B cell). The myeloid populations
501 (macrophages and neutrophils) were selected and reclustered into more fine-grained populations
502 using the same strategy as above.
503
504 Data from Silvin, et al.(12) were retrieved from the European Genome Archive (EGA) under
505 accession number E-MTAB-9221 as FASTQ files. Sequencing data were processed as detailed
506 above for PRJNA608742, using the same parameters for identifying cellular droplets and filtering
507 droplets with high mitochondrial RNA abundance. Normalization, clustering and manual
508 annotation was performed as described above. Count data from Delorey, et al.(5) were downloaded
509 from the Broad Single Cell Portal using accession number SCP1052. We used the cell annotations
510 as defined within that dataset, selecting cells labeled as Myeloid using the Cluster field defined by
511 the authors. Data from Grant, et al.(6) were retrieved from the Gene Expression Omnibus (GEO)
512 under accession number GSE155249. Normalization and clustering were performed as above.
513 Annotations from the original publication were used to group cells into broad lineages: epithelial
514 cells, B cells, T cells, dendritic cells, mast cells, macrophages and mixed myeloid cells.
515
516 *Pseudobulk expression profile calculation*

517 The aggregateAcrossCells method from the scater R package(57) was used to calculate pseudobulk
518 expression profiles for each cell population in a sample. This method uses the sum of raw counts
519 to determine an estimate of the aggregate expression of that cell type in a sample. The TMM
520 method from the edgeR R package(60) was used to normalize the pseudobulk count data within
521 each dataset. Signature score calculation in pseudo-bulk data was performed as previously
522 described(61) using the GSDecon package (https://github.com/JasonHackney/GSDecon).
523

524 *COMET PBMC CITE-seq analysis*

525 The raw scRNA-seq counts were normalized using the 'LogNormalized' method implemented in
526 the 'NormalizeData' function from the Seurat R package(62); with this method, the feature counts
527 are divided by the total counts for each cell, multiplied by a scale factor of 10,000, and then natural-
528 log transformed. The raw ADT counts were normalized using the 'CLR' method implemented in
529 Seurat's 'NormalizeData' function; with this method, a centered log ratio transformation is
530 applied. The ENRAGE and MS1 gene set scores were calculated for each cell using the
531 'score_genes' function implemented in the scanpy Python package(63). All of the pseudobulk
532 values for each cell population in a sample (i.e., sample + cell type)—that is, the mRNA
533 expression, ADT expression, and gene set scores—were calculated as the average across all cells
534 in that population. Correlations between gene set scores and ADT expression were on pseudobulk
535 data and refer to a population of cells across patients.
536

537 *Identification of EN-RAGE gene expression induced by IL-6 in vitro.*

538 PBMCs were isolated from 50 mL of heparinized blood of four healthy donors by Ficoll-Paque.
539 Primary human monocytes were purified from PBMC by Miltenyi Pan Monocyte Isolation Kit and

540 cultured in RPMI with 10% heat-inactivated FBS, 10 mM HEPES and L-glutamine. The primary
541 human monocytes were stimulated with 10 ng/mL IL-6 + 18.7 ng/mL IL6R for 24 hours, and
542 RNA-seq performed on bulk cells. Unsupervised clustering using average linkage cluster
543 difference and Euclidean point distance metrics were used to generate heat maps. RNA was
544 isolated using the Qiagen RNeasy 96 kit (Qiagen catalog: 74182). Total RNA was quantified with
545 Qubit RNA HS Assay Kit (Thermo Fisher Scientific catalog: Q32852) and quality was assessed
546 using RNA ScreenTape on 4200 TapeStation (Agilent Technologies catalog: 5067-5576). cDNA
547 library was generated from 2 nanograms of total RNA using Smart-Seq V4 Ultra Low Input RNA
548 Kit (Takara catalog: 634894). 150 picograms of cDNA was used to make sequencing libraries by
549 Nextera XT DNA Sample Preparation Kit (Illumina catalog: FC-131-1024). Libraries were
550 quantified with Qubit dsDNA HS Assay Kit (Thermo Fisher Scientific catalog: Q32851) and the
551 average library size was determined using D1000 ScreenTape on 4200 TapeStation (Agilent
552 Technologies catalog: 5067-5582). Libraries were pooled and sequenced on the Illumina NovaSeq
553 6000 to generate 30 million single-end 50 base pair reads for each sample. Sequencing reads were
554 filtered and aligned using HTSeqGenie v4.4.2(64). GSNAP v2013-11-01 was used for alignment,
555 through the HTSeqGenie wrapper, against the GENCODE 27 Basic gene model on the human
556 genome assembly GRCh38. Only reads with unique genomic alignments were analyzed.
557 Normalized CPM (Counts Per Million) were used as a normalized measure of gene expression,
558 calculated using method provided in edgeR(60).
559

560 *COMET cohort*

561 The COVID-19 Multi-Phenotyping for Effective Therapies (COMET) cohort collected PBMCs,
562 whole blood, ETA and plasma longitudinally from hospitalized patients presenting with COVID-

563 19 symptoms. This study included 75 patients with samples collected in 2020, of whom 57 were
564 positive (76%) for SARS-CoV-2, along with 11 healthy controls(2, 36, 37). Table 1 summarizes
565 the patient characteristics. All-cause mortality occurred within 30 days for 9 of 10 subjects.
566 Ventilator-free days (VFDS) were assessed at D28, with fatal cases assigned 0. NIH COVID-19
567 ordinal severity score and Sequential Organ Failure Assessment (SOFA) scores were assessed at
568 study enrollment (Day 0), when baseline samples were collected, with a 9 day median time from
569 symptom onset (4-13 IQR). Severity groups were defined as follows. PBMC: Moderate = no
570 supplemental O_2, severe = supplemental O_2 and critical = mechanical ventilation. Whole blood:
571 Mild/Moderate = 0 days on ventilator and no more than 1 day in ICU, Severe patients had ≥1 day
572 on ventilator. ETA: Critical=VFDS=0 (ventilation for ≥28 days or death), severe ETA=VFDS>0.
573

574 PBMCs were isolated and single cell RNA sequencing and Cellular Indexing of Transcriptomes
575 and Epitopes by Sequencing (CITE-seq) data was generated as previously described(37), with cell
576 types defined by marker genes. The complete protocol is available on protocols.io
577 (https://www.protocols.io/view/10x-citeseq-protocol-covid-19-patient-samples-tetr-bqnqmvdw).
578 Data was generated for 188 unique cell surface antigens. CITE-seq data was included from 128
579 samples collected at day 0, day 7 and/or day 14 from 60 patients. Single cell RNA-seq data
580 generated from PBMC collected at day 0 from 49 patients, whole blood collected at day 0 for 18
581 patients, and 41 ETA samples collected longitudinally from 16 patients were included in this study.
582 Bulk gene expression data was generated from 182 samples collected longitudinally from 19
583 patients. Plasma cytokine and paired ETA scRNA-seq data was available for only 7 samples,
584 precluding correlation analyses.
585

586 *COVACTA tocilizumab clinical trial*

587 A total of 438 hospitalized COVID-19 patients were randomized 2:1 for anti-interleukin-6 receptor
588 antibody, tocilizumab, or placebo and included in the modified intention to treat population
589 (tocilizumab: 294, placebo: 144). Hospitalized patients were ≥18 years of age with COVID-19
590 pneumonia confirmed by a positive SARS-CoV-2 PCR test and evidenced by x-ray or computed
591 tomography (CT) scan. Eligible patients had a blood oxygen saturation of ≤93% or partial pressure
592 of oxygen/fraction of inspired oxygen of <300 mm/Hg. Details of the COVACTA study design
593 have been published (Clinical trials.gov NCT04320615)(34). Population demographics for the 404
594 patients with available blood RNA-seq data are described in Table 1.

595

596 Serum IL-6 was quantified using a validated in vitro diagnostic method (Roche Cobas; Roche
597 Diagnostics, Indianapolis, IN) at central laboratories (PPD). Complete blood counts were
598 measured using standard clinical chemistry and haematology methods available at local hospital
599 laboratories. IFNγ and IL10 were measured by qualified immunoassays (Simpleplex,
600 ProteinSimple, San Jose, CA, USA) at central laboratories (Covance). The Olink Explore platform
601 was used to measure 1472 serum proteins (Olink, Uppsala, Sweden). RNA was isolated from blood
602 PaxGene (Qiagen, Hilden Germany) samples by Q2 Solutions. 1.25 ug of RNA was used for
603 generating sequencing libraries with the TruSeq® Stranded mRNA Library Prep kit (Illumina, San
604 Diego, CA, USA). The libraries were sequenced by Illumina NovaSeq by 50 bp single-end reads
605 at a read depth of 50 million reads per sample.

606

607 For the time point comparisons (D1 to D7) patients were subset to those subjects with
608 measurements at both time points before differential expression analysis with DESeq2. Unfiltered

609 DESeq2 outputs were ranked by log2 fold change and then the FGSEA Bioconductor package was
610 used to calculate enrichment scores. We used the ggplot2 package to generate visualizations. T
611 cell genes with a relationship to EN-RAGE state in COMET scRNA-seq data were examined in
612 COVACTA, and limited to the subset of T cell suppressive genes that were predominantly
613 expressed by T cells in COMET whole blood transcriptome data to permit analysis of bulk gene
614 expression data. Computational methods are described in more detail elsewhere(14).
615

616 *COVID-19 clinical severity*

617 Within the COVACTA clinical trial, the NIH COVID-19 ordinal severity scale was used to assess
618 disease severity: 3=hospitalized not requiring supplemental O_2, 4= supplemental O_2, 5= non-
619 invasive/high flow O_2, 6= mechanical ventilation, 7= mechanical ventilation + additional organ
620 support (eg, vasopressors, renal replacement therapy, ECMO), 8=death. In the COMET cohort of
621 PBMC samples, moderate = no supplemental O_2 (NIH ordinal scale 3-4), severe = supplemental
622 O_2 (5-6) and critical = mechanical ventilation (7). The maximal NIH ordinal severity scale recorded
623 during hospitalization was calculated for each patient in COMET. Ventilator-free days were
624 calculated over 28 days, with fatal patients scored as 0. ARDS was diagnosed using the American-
625 European Consensus Conference (AECC) definition(65) or Berlin definition(66). The sequential
626 organ failure assessment (SOFA) score was calculated at study enrollment.
627

628 *Statistical analysis*

629 Gene expression was $\log_2$ normalized. Patient demographics are given as median (IQR) and
630 frequency (%). Medians and first and third quartile ranges are shown in box and whisker plots and
631 medians are shown on dot plots. Longitudinal COVACTA line plots show means and 95%

632 confidence intervals. Two-sided unpaired t-tests were used to compare gene signature scores
633 between cell types in pseudobulk scRNA-seq data. Student's t-test was used to calculate p values
634 for comparisons of EN-RAGE gene set scores and clinical severity. A mixed linear model was
635 used to compare slopes of longitudinal EN-RAGE gene set expression between severity groups.
636 Spearman correlations and two-tailed p values were calculated to examine relationships between
637 biomarkers and clinical severity and EN-RAGE gene set vs. myeloid gene expression. False
638 discovery rates were calculated for differential expression analysis of bulk RNAseq data
639 (accounting for transcriptome-wide analysis of x genes), GSEA (accounting for the x gene sets
640 analyzed), and COMET PBMC CITE-seq data (accounting for 188 measured proteins), using the
641 Benjamini-Hochberg method. Biorenderer was used to generate some Figures.
642

643 *Study approval*

644 The COMET study was approved by the Institutional Review Board: UCSF Human Research
645 Protection Program (HRPP) IRB# 20-30497 and informed consent was obtained for patients.
646 COVACTA was conducted in accordance with Good Clinical Practice guidelines of the
647 International Council for Harmonisation E6 and the Declaration of Helsinki or local laws and
648 regulations, whichever afforded greater protection. Informed consent was obtained from the
649 patient or their legally authorized representative prior to participation. The studies were approved
650 by institutional review boards or ethics committees at each site.
651

652 **Data availability**
653

654 The RNAseq and proteomics data that support the findings of this study are available in the public
655 online respositories Gene Expression Omnibus (GEO), SRA, and the European Genome-Phenome

656 Archive (EGA). COMET: GEO GSE163668 (whole blood), GSE163426 (tracheal aspirate),
657 GSE168453 (PBMC). Schulte-Schrepping, et al.: http://fastgenomics.org. Liao, et al.: SRA
658 PRJNA608742. Silvin, et al.: EGA E-MTAB-9221. Delorey, et al.: Broad Single Cell Portal
659 accession number SCP1052. Grant, et al.: GEO GSE155249. COVACTA RNA-seq, proteomics,
660 and clinical metadata: EGA; accession number EGAS00001006688 (available to qualified
661 researchers upon request; https://ega-archive.org/). Individual patient level clinical data for the
662 COVACTA study is available through the clinical study data request platform (https://vivli.org/).
663

664 **Code availability**

665 No new algorithms were developed for this manuscript. Most of the analyses performed in this
666 study used published packages mentioned in the Methods, with the exception of the
667 EnhancedVolcano (https://github.com/kevinblighe/EnhancedVolcano) package used to generate
668 volcano plots. All code generated for analysis is available from the authors upon request.
669

670 **Author Contributions**

671 C.M.R., J.A.H, and H.S. conceived of and designed the overall study. J.A.H., H.S., H.VH., C.O.,
672 L.O., X.G., A.C., and C.M.R. performed and interpreted computational analyses. X.G. performed
673 *in vitro* experiments. X.G., N.W., A.Q., D.C., A.C., D.F.C., A.J.C., T.C., G.K.F., A.A.R., A.R.,
674 J.T., K.H., N.F.K., M.F.K., D.J.E., K.K., A.S., Z.L., C.S.C., P.G.W., R.G., E.M., A.B., B.S.Z.,
675 C.L., C.M.H., M.G.P.vdW, G.C.H., T.G., R.B., D.S.L., J.R.G., Y.S., R.P., A.O., A.W., C.J.Y.,
676 UCSF COMET Consortium, T.R., J.M.M., F.C., A.T., M.B., L.T., I.O.R., A.R., S.B.K., R.N.B.,
677 C.M.R. facilitiated the COMET or COVACTA studies and providing data and/or critical feedback
678 on methods and results. C.M.R., J.A.H, and H.S. wrote the first draft of the manuscript. J.A.H is

679 listed first for defining the ENRAGE signature and responsible for analysis of COMET and public
680 datasets, with H.S. responsible for analysis of the COVACTA study. All authors reviewed and
681 approved the final manuscript.

682

683 **Acknowledgements**

684 This study was supported with funding from Roche, Inc. and federal funds from the Department
685 of Health and Human Services; Office of the Assistant Secretary for Preparedness and Response;
686 Biomedical Advanced Research and Development Authority, under OT number:
687 HHSO100201800036C. C.J.Y. is further supported by the NIH grants R01AR071522,
688 R01AI136972, U01HG012192, and the Chan Zuckerberg Initiative, and is an investigator at the
689 Chan Zuckerberg Biohub and is a member of the Parker Institute for Cancer Immunotherapy
690 (PICI). G.C.H. was supported by the National Science Foundation Undergraduate Research
691 Fellowship Program 1650113. C.S.C. is further supported by NIH R35HL140026. C.H. is further
692 supported by a K23 from NHLBI K23 HL133495.

693

694 UCSF COMET Consortium co-authors: Yumiko Abe-Jones, Michael Adkisson, K. Mark Ansel,
695 Saurabh Asthana, Alexander Beagle, Sharvari Bhide, Cathy Cai, Saharai Caldera, Maria Calvo,
696 Sidney A. Carrillo, Suzanna Chak, Stephanie Christenson, Zachary Collins, Spyros Darmanis,
697 Angela Detweiler, Catherine DeVoe, Walter Eckalbar, Jeremy Giberson, Ana Gonzalez, Gracie
698 Gordon, Paula Hayakawa Serpa, Alejandra Jauregui, Chayse Jones, Serena Ke, Divya Kushnoor,
699 Tasha Lea, Deanna Lee, Aleksandra Leligdowicz, Yale Liu, Salman Mahboob, Lenka Maliskova,
700 Michael Matthay, Elizabeth McCarthy, Priscila Muñoz-Sandoval, Norma Neff, Viet Nguyen,
701 Nishita Nigam, Randy Parada, Maira Phelps, Logan Pierce, Priya Prasad, Sadeed Rashid, Gabriella
702 Reeder, Nicklaus Rodriguez, Bushra Samad, Andrew Schroeder, Cole Shaw, Alan Shen, Austin

Sigman, Pratik Sinha, Matthew Spitzer, Sara Sunshine, Kevin Tang, Luz Torres Altamirano, Alexandra Tsitsiklis, Erden Tumurbaatar, Vaibhav Upadhyay, Alexander Whatley, Andrew Willmore, Michael Wilson, Juliane Winkler, Kristine Wong, Kimberly Yee, Michelle Yu, Mingyue Zhou, Wandi S. Zhu

References

1. Arunachalam PS et al. Systems biological assessment of immunity to mild versus severe COVID-19 infection in humans. *Science (1979)* 2020;369(6508):1210–1220.

2. Combes AJ et al. Global absence and targeting of protective immune states in severe COVID-19. *Nature* 2021;591(7848):124–130.

3. Zheng H et al. Multi-cohort analysis of host immune response identifies conserved protective and detrimental modules associated with severity across viruses [Internet]. *Immunity* 2021;54(4):753-768.e5.

4. MacDonald L et al. COVID-19 and RA share an SPP1 myeloid pathway that drives PD-L1+ neutrophils and CD14+ monocytes [Internet]. *JCI Insight* 2021;6(13). doi:10.1172/jci.insight.147413

5. Delorey TM et al. COVID-19 tissue atlases reveal SARS-CoV-2 pathology and cellular targets [Internet]. *Nature* 2021;595(7865):107–113.

6. Grant RA et al. Circuits between infected macrophages and T cells in SARS-CoV-2 pneumonia [Internet]. *Nature* 2021;590(7847):635–641.

7. Liao M et al. Single-cell landscape of bronchoalveolar immune cells in patients with COVID-19 [Internet]. *Nat Med* 2020;26(6):842–844.

8. Ren X et al. COVID-19 immune features revealed by a large-scale single-cell transcriptome atlas [Internet]. *Cell* 2021;184(7):1895-1913.e19.

9. Reyes M et al. An immune-cell signature of bacterial sepsis [Internet]. *Nat Med* 2020;26(3):333–340.

10. Reyes M et al. Plasma from patients with bacterial sepsis or severe COVID-19 induces suppressive myeloid cell production from hematopoietic progenitors in vitro. [Internet]. *Sci Transl Med* 2021;13(598):9599.

11. Schulte-Schrepping J et al. Severe COVID-19 Is Marked by a Dysregulated Myeloid Cell Compartment. [Internet]. *Cell* 2020;182(6):1419-1440.e23.

12. Silvin A et al. Elevated Calprotectin and Abnormal Myeloid Cell Subsets Discriminate Severe from Mild COVID-19 [Internet]. *Cell* 2020;182(6):1401.

13. Rowlands M, Segal F, Hartl D. Myeloid-Derived Suppressor Cells as a Potential Biomarker and Therapeutic Target in COVID-19. *Front Immunol* 2021;12:2435.

14. Shivram H et al. Tocilizumab treatment leads to early resolution of myeloid dysfunction and lymphopenia in patients hospitalized with COVID-19 [Internet]. *bioRxiv* 2022;2022.10.27.514096.

15. LaSalle TJ et al. Longitudinal characterization of circulating neutrophils uncovers distinct phenotypes associated with severity in hospitalized COVID-19 patients [Internet]. *Cell Rep Med* 2022;3(10):100779.

16. Stephenson E et al. Single-cell multi-omics analysis of the immune response in COVID-19 [Internet]. *Nat Med* 2021;27(5):904–916.

17. Bost P et al. Deciphering the state of immune silence in fatal COVID-19 patients [Internet]. *Nat Commun* 2021;12(1):1428.

742 18. Kvedaraite E et al. Major alterations in the mononuclear phagocyte landscape associated with COVID-19 severity.
743 [Internet]. *Proc Natl Acad Sci U S A* 2021;118(6). doi:10.1073/pnas.2018587118
744 19. Schrijver IT, Théroude C, Roger T. Myeloid-Derived Suppressor Cells in Sepsis [Internet]. *Front Immunol*
745 2019;10:327.
746 20. Gabrilovich DI, Nagaraj S. Myeloid-derived suppressor cells as regulators of the immune system [Internet]. *Nature*
747 *Reviews Immunology 2009 9:3* 2009;9(3):162–174.
748 21. Veglia F, Sanseviero E, Gabrilovich DI. Myeloid-derived suppressor cells in the era of increasing myeloid cell
749 diversity. *Nat Rev Immunol* 2021;21(8):485–498.
750 22. Hegde S, Leader AM, Merad M. MDSC: Markers, development, states, and unaddressed complexity [Internet].
751 *Immunity* 2021;54(5):875–884.
752 23. Agrati C et al. Expansion of myeloid-derived suppressor cells in patients with severe coronavirus disease (COVID-19)
753 [Internet]. *Cell Death Differ* 2020;27:3196–3207.
754 24. Darcy CJ et al. Neutrophils with myeloid derived suppressor function deplete arginine and constrain T cell function in
755 septic shock patients [Internet]. *Crit Care* 2014;18(4):R163.
756 25. Dean MJ et al. Severe COVID-19 Is Characterized by an Impaired Type I Interferon Response and Elevated Levels of
757 Arginase Producing Granulocytic Myeloid Derived Suppressor Cells. [Internet]. *Front Immunol* 2021;12:695972.
758 26. Falck-Jones S et al. Functional monocytic myeloid-derived suppressor cells increase in blood but not airways and
759 predict COVID-19 severity [Internet]. *Journal of Clinical Investigation* 2021;131(6). doi:10.1172/JCI144734
760 27. Reizine F et al. SARS-CoV-2-Induced ARDS Associates with MDSC Expansion, Lymphocyte Dysfunction, and
761 Arginine Shortage. *J Clin Immunol* 2021;41(3):515–525.
762 28. Sacchi A et al. Early expansion of myeloid-derived suppressor cells inhibits SARS-CoV-2 specific T-cell response and
763 may predict fatal COVID-19 outcome [Internet]. *Cell Death Dis* 2020;11(10):921.
764 29. Tom J et al. Prognostic and Predictive Biomarkers in Patients with Coronavirus Disease 2019 Treated with
765 Tocilizumab in a Randomized Controlled Trial∗ [Internet]. *Crit Care Med* 2022;50(3):398–409.
766 30. Bunt SK et al. Reduced Inflammation in the Tumor Microenvironment Delays the Accumulation of Myeloid-Derived
767 Suppressor Cells and Limits Tumor Progression [Internet]. *Cancer Res* 2007;67(20):10019.
768 31. Chen G et al. Clinical and immunological features of severe and moderate coronavirus disease 2019 [Internet]. *J Clin*
769 *Invest* 2020;130(5):2620–2629.
770 32. Oh K et al. A mutual activation loop between breast cancer cells and myeloid-derived suppressor cells facilitates
771 spontaneous metastasis through IL-6 trans-signaling in a murine model [Internet]. *Breast Cancer Research*
772 2013;15(5):R79.
773 33. Weber R et al. IL-6 as a major regulator of MDSC activity and possible target for cancer immunotherapy. *Cell*
774 *Immunol* 2021;359:104254.

775 34. Rosas IO et al. Tocilizumab in Hospitalized Patients with Severe Covid-19 Pneumonia [Internet]. *N Engl J Med*
776 2021;384(16):1503–1516.
777 35. Shankar-Hari M et al. Association Between Administration of IL-6 Antagonists and Mortality Among Patients
778 Hospitalized for COVID-19: A Meta-analysis [Internet]. *JAMA* 2021;326(6):499–518.
779 36. Sarma A et al. Tracheal aspirate RNA sequencing identifies distinct immunological features of COVID-19 ARDS
780 [Internet]. *Nature Communications 2021 12:1* 2021;12(1):1–10.
781 37. van der Wijst MGP et al. Type I interferon autoantibodies are associated with systemic immune alterations in patients
782 with COVID-19 [Internet]. *Sci Transl Med* 2021;13(612):eabh2624.
783 38. Su Y et al. Multi-Omics Resolves a Sharp Disease-State Shift between Mild and Moderate COVID-19 [Internet]. *Cell*
784 2020;183(6):1479.
785 39. Aschenbrenner AC et al. Disease severity-specific neutrophil signatures in blood transcriptomes stratify COVID-19
786 patients [Internet]. *Genome Medicine 2021 13:1* 2021;13(1):1–25.
787 40. Hasegawa T et al. The regulation of EN-RAGE (S100A12) gene expression in human THP-1 macrophages [Internet].
788 *Atherosclerosis* 2003;171(2):211–218.
789 41. Lorenz E et al. Different expression ratio of S100A8/A9 and S100A12 in acute and chronic lung diseases. *Respir Med*
790 2008;102(4):567–573.
791 42. Medina E, Hartl D. Myeloid-Derived Suppressor Cells in Infection: A General Overview [Internet]. *J Innate Immun*
792 2018;10(5–6):407–413.
793 43. Eisemann T, Costa B, Peterziel H, Angel P. Podoplanin Positive Myeloid Cells Promote Glioma Development by
794 Immune Suppression [Internet]. *Front Oncol* 2019;9(MAR):187.
795 44. Karakasheva TA et al. CD38-expressing myeloid-derived suppressor cells promote tumor growth in a murine model of
796 esophageal cancer [Internet]. *Cancer Res* 2015;75(19):4074–4085.
797 45. Newman AM et al. Robust enumeration of cell subsets from tissue expression profiles [Internet]. *Nature Methods 2015*
798 *12:5* 2015;12(5):453–457.
799 46. Zhou R et al. Acute SARS-CoV-2 Infection Impairs Dendritic Cell and T Cell Responses [Internet]. *Immunity*
800 2020;53(4):864.
801 47. Meckiff BJ et al. Imbalance of Regulatory and Cytotoxic SARS-CoV-2-Reactive CD4+ T Cells in COVID-19
802 [Internet]. *Cell* 2020;183(5):1340.
803 48. Files JK et al. Sustained cellular immune dysregulation in individuals recovering from SARS-CoV-2 infection
804 [Internet]. *J Clin Invest* 2021;131(1). doi:10.1172/JCI140491
805 49. Wilk AJ et al. A single-cell atlas of the peripheral immune response in patients with severe COVID-19. *Nat Med*
806 2020;26(7):1070–1076.
807 50. Diao B et al. Reduction and Functional Exhaustion of T Cells in Patients With Coronavirus Disease 2019 (COVID-19)
808 [Internet]. *Front Immunol* 2020;11:827.

809 51. Mathew D et al. Deep immune profiling of COVID-19 patients reveals distinct immunotypes with therapeutic
810 implications. *Science (1979)* 2020;369(6508). doi:10.1126/SCIENCE.ABC8511
811 52. Zheng M et al. Functional exhaustion of antiviral lymphocytes in COVID-19 patients [Internet]. *Cell Mol Immunol*
812 2020;17(5):533–535.
813 53. Galván-Peña S et al. Profound Treg perturbations correlate with COVID-19 severity [Internet]. *Proceedings of the*
814 *National Academy of Sciences* 2021;118(37):e2111315118.
815 54. Fahey E, Doyle SL. IL-1 Family Cytokine Regulation of Vascular Permeability and Angiogenesis [Internet]. *Front*
816 *Immunol* 2019;10(JUN):1426.
817 55. Pittet J-F et al. TGF-β is a critical mediator of acute lung injury [Internet]. *Journal of Clinical Investigation*
818 2001;107(12):1537.
819 56. R Core Team. R: A language and environment for statistical computing. [Internet]. *R Foundation for Statistical*
820 *Computing, Vienna, Austria*. [published online ahead of print: 2020];https://www.r-project.org. cited
821 57. McCarthy D, Campbell K, Lun A, Wills Q. scater: pre-processing, quality control, normalisation and visualisation of
822 single-cell RNA-seq data in R [Internet]. *Scater: Pre-processing, quality control, normalization and visualization of*
823 *single-cell RNA-seq data in R* 2016;069633.
824 58. Lun ATL, McCarthy DJ, Marioni JC. A step-by-step workflow for low-level analysis of single-cell RNA-seq data with
825 Bioconductor [Internet]. *F1000Res* 2016;5. doi:10.12688/f1000research.9501.2
826 59. Lun ATL et al. EmptyDrops: Distinguishing cells from empty droplets in droplet-based single-cell RNA sequencing
827 data [Internet]. *Genome Biol* 2019;20(1):1–9.
828 60. Robinson MD, McCarthy DJ, Smyth GK. edgeR: a Bioconductor package for differential expression analysis of digital
829 gene expression data [Internet]. *Bioinformatics* 2010;26(1):139–140.
830 61. Bueno R et al. Comprehensive genomic analysis of malignant pleural mesothelioma identifies recurrent mutations,
831 gene fusions and splicing alterations [Internet]. *Nature Genetics 2016 48:4* 2016;48(4):407–416.
832 62. Hao Y et al. Integrated analysis of multimodal single-cell data [Internet]. *Cell* 2021;184(13):3573-3587.e29.
833 63. Wolf FA, Angerer P, Theis FJ. SCANPY: large-scale single-cell gene expression data analysis [Internet]. *Genome Biol*
834 2018;19(1):15.
835 64. Pau G RJ. HTSeqGenie: A NGS analysis pipeline.. *R package version 4.22.0*. 2013;
836 65. Bernard GR et al. The American-European Consensus Conference on ARDS. Definitions, mechanisms, relevant
837 outcomes, and clinical trial coordination. [Internet]. *Am J Respir Crit Care Med* 1994;149(3):818–824.
838 66. Ranieri VM et al. Acute respiratory distress syndrome: The Berlin definition [Internet]. *JAMA - Journal of the*
839 *American Medical Association* 2012;307(23):2526–2533.
840 67. Angelova M et al. Characterization of the immunophenotypes and antigenomes of colorectal cancers reveals distinct
841 tumor escape mechanisms and novel targets for immunotherapy [Internet]. *Genome Biology 2015 16:1* 2015;16(1):1–17.
842

Tables

Table 1. Patient characteristics

NA = not available. COVACTA data are for subjects with blood RNA-seq data included in this manuscript. COVACTA ICU admission frequency is at time of baseline sampling.

	COMET			COVACTA
	All	SARS-CoV-2+	SARS-CoV-2-	
n (%)	75	57 (76%)	18 (24%)	404
Age median (IQR)	54 (42, 69)	48 (42, 66)	66 (51, 76)	63 (53-70)
Sex				
Male n (%)	52 (69%)	43 (75%)	9 (50%)	284 (70%)
Female n (%)	23 (31)	14 (25%)	9 (50%)	120 (30%)
Race n (%)				
White	20 (27%)	11 (19%)	9 (50%)	233 (58%)
Black/African American	4 (5%)	3 (5%)	1 (6%)	58 (14%)
Asian	13 (17%)	9 (16%)	4 (22%)	37 (9%)
Other/Mixed/Unknown	38 (51%)	34 (60%)	4 (22%)	76 (19%)
Baseline NIH Ordinal Scale n (%)				
3 No supplemental O2	14 (19%)	12 (21%)	2 (11%)	15 (4%)
4 Supplemental O2	25 (33%)	18 (32%)	7 (39%)	109 (27%)
5 Non-invasive/high flow O2	14 (19%)	9 (16%)	5 (28%)	114 (28%)
6 Mechanical ventilation (MV)	3 (4%)	3 (5%)	0 (0%)	58 (14%)
7 MV + additional organ support	19 (25%)	15 (26%)	4 (22%)	107 (27%)
SOFA maximal median (IQR)	4 (1, 10)	4 (1, 11)	4 (1, 9)	NA
ICU admission n (%)	26 (35%)	30 (53%)	11 (61%)	234 (58%)
Mortality n (%)	10 (13%)	6 (11%)	4 (22%)	83 (20%)
ARDS AECC definition n (%)	38 (51%)	26 (46%)	12 (67%)	NA
ARDS Berlin definition n (%)	23 (31%)	18 (32%)	5 (28%)	NA
Hospitalization, days median (IQR)	8 (8, 18)	11 (3, 20)	5 (4, 7)	22 (9-28)
ICU duration, days median (IQR)	2 (0, 9)	14 (4, 26)	4 (2, 4)	14 (0-27)
Ventilator-free days median (IQR)	28 (18, 28)	28 (16, 28)	28 (26, 28)	19 (0-28)

Figures

Figure 1. Identification of the severity-associated EN-RAGE myeloid signature in COVID-19 airway (BAL) and peripheral (PBMC) samples.
A. Pairwise Pearson correlation between all genes and S100A12 in either PBMC(11) or BAL(7).
B. Pseudo-bulk expression profiles of PBMC and BAL. Each point represents a patient. Blue=healthy (BAL n = 3; PBMC, n = 3), yellow=moderate/severe (BAL, n = 3; PBMC, n = 8; hospitalized -/+ supplemental O_2), red=critical (BAL, n = 6; PBMC, n = 10; requiring mechanical ventilation), with severity defined within each dataset by the authors. Increased expression in severe patients in both tissues. Significance was tested using a t-test across the indicated groups (n.s. = $p > 0.05$, * = $p < 0.05$; ** = $p < 0.01$; *** = $p < 0.001$).

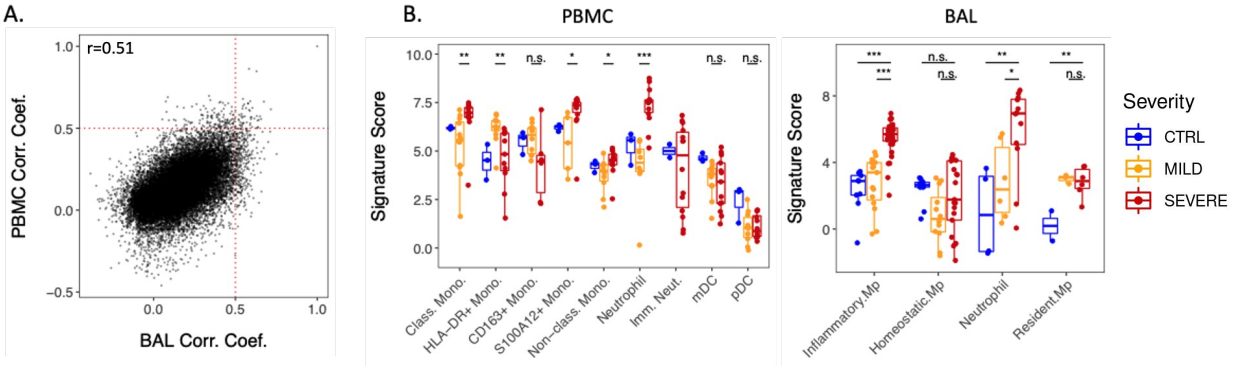

Figure 2. Replication of EN-RAGE severity association across sample types in both COVID-19 and non-COVID-19 acute lung injury (COMET cohort).

A. UMAP plots with cell type annotations. Each point represents a single cell, colored by cell type. Each panel shows a different sample type, as indicated. PBMC: peripheral blood mononuclear cells, WB: whole blood, ETA:endotracheal aspirates.

B. UMAP plots showing EN-RAGE signature score. Each point represented a single cell colored by the expression signature value.

C. Pseudo-bulk expression profiles within myeloid cells. Each point represents the pseudo-bulk gene expression signature score for a cell type in a patient sample. PBMC severity: Moderate = no supplemental O_2, severe = supplemental O_2 and critical = mechanical ventilation. Whole blood severity: Mild/Moderate = 0 days on ventilator and no more than 1 day in ICU, Severe patients had ≥1 day on ventilator. ETA: Critical=VFDS=0 (ventilation for ≥28 days or death), severe ETA=VFDS>0. Significance was tested using a t-test across the indicated groups (n.s. = $p > 0.05$, ** = $p < 0.01$; *** = $p < 0.001$). Sample numbers per cohort: PBMC healthy, n = 11; PBMC COVID- moderate, n = 4; PBMC COVID- severe, n = 6; PBMC COVID- critical, n = 3; PBMC COVID+ moderate, n = 12; PBMC COVID+ severe, n = 10; PBMC COVID+ critical, n = 14. WB healthy, n = 14; WB COVID- mild, n = 4; WB COVID- severe, n = 1; WB COVID+ mild, n = 8; WB COVID+ severe, n = 5. ETA COVID- moderate/severe, n = 2; ETA COVID- critical, n = 1; ETA COVID+ moderate/severe, n = 5; ETA COVID+ critical, n = 8.

885

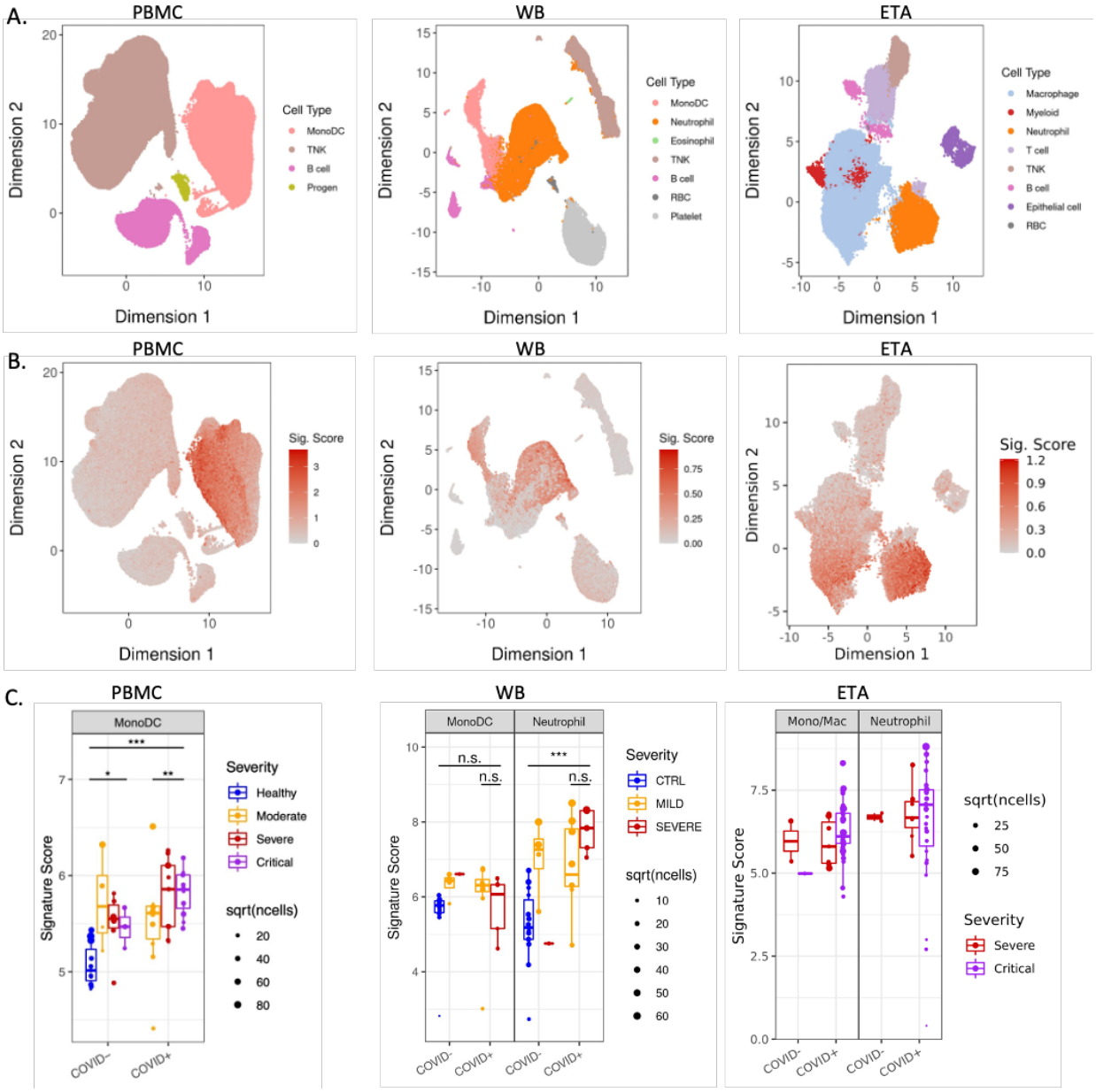
A.
PBMC
WB
ETA
Dimension 1
Dimension 2
Cell Type
MonoDC
TNK
B cell
Progen
Neutrophil
Eosinophil
RBC
Platelet
Macrophage
Myeloid
T cell
Epithelial cell
B.
Sig. Score
C.
Signature Score
MonoDC
Neutrophil
Mono/Mac
Severity
Healthy
Moderate
Severe
Critical
CTRL
MILD
SEVERE
sqrt(ncells)
COVID-
COVID+
n.s.

886

887 **Figure 3.** EN-RAGE signature expression correlates with disease severity and immunosuppressive
888 gene expression in myeloid cells (COMET cohort).
889 **A.** Spearman correlations between pseudo-bulk EN-RAGE signature score in PBMC monocytes
890 and NIH ordinal severity score, maximal NIH severity score, SOFA organ failure score, and
891 plasma IL-6 and IL-10 protein levels at study enrollment. **B.** PBMC monocyte EN-RAGE gene
892 score is higher in patients who develop ARDS (AECC definition) in COVID-19 patients; n=46.
893 Medians are indicated. * t-test $p<0.05$. **C.** Longitudinal changes in EN-RAGE signature in bulk
894 ETA RNA-seq. Each point represents a patient sample from COVID-19 (n=16 patients, n=276
895 samples) and non-COVID (n=3 patients, n=6 samples) patients requiring mechanical ventilation.
896 Samples from the same patient are linked by dotted lines. Points are colored by severity of disease.
897 For illustrative purposes, linear regression trend lines for signature scores over time, grouped by
898 severity level are shown as solid lines. Slopes were significantly different using a linear mixed
899 model, $p<0.05$. MV=mechanical ventilation. **D.** Table of Spearman correlation coefficients
900 between pseudo-bulk EN-RAGE signature score and genes encoding myeloid effector functions
901 within monocyte or neutrophil populations across endotracheal aspirates (ETA), whole blood, and
902 PBMCs from the COMET cohort. Positive correlations are shaded red and negative correlations
903 shaded blue, with increasing darkness of shading indicating two tailed p values of $p<0.05$, $p<0.01$,
904 and $p<0.001$. **E.** PBMC myeloid EN-RAGE gene score correlates with plasma IL-6 and IL-10
905 protein; n=46. **F.** Correlation of pseudo-bulk expression signature for EN-RAGE genes compared
906 to pseudo-bulk expression values of IL-10 and PD-L1 in monocytes in COMET tracheal aspirate
907 samples. Each point represents the expression value in a cell type in a single sample; n=40. Log_2
908 gene expression, Spearman correlation coefficients and two tailed p values are shown.
909

A

		Clinical severity		Clinical outcome		Plasma protein	
PBMC		NIH	SOFA	NIH MAX	VFDS	IL-6	IL-10
Monocyte	r	0.37	0.22	0.30	-0.25	0.41	0.29
	p	0.010	0.15	0.02	0.10	0.005	0.05

B

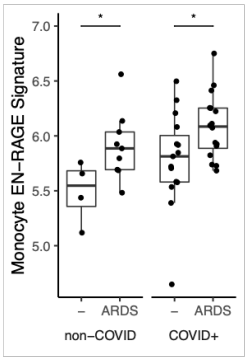

C

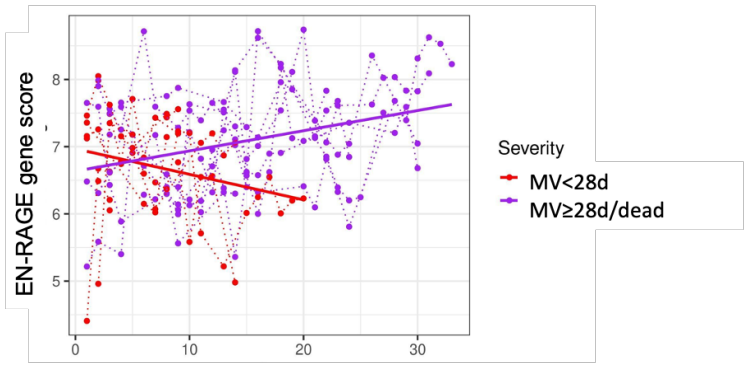

D

		Lung recruitment/phenotype						T cell suppression					
Spearman rho		HLA.DRA	HLA.DRB1	CD14	CCR2	PTGER2	STAT3	ENRAGE	IL10	PDL1	IL1B	CYBB	TGFB1
ETA	n												
Monocyte	41	0.11	-0.23	0.09	0.26	0.72	0.75	0.70	0.74	0.59	0.86	0.14	0.13
Neutrophil	40	0.03	-0.16	0.58	0.00	0.35	0.63	0.74	0.53	0.59	0.78	0.21	0.54
Blood	n												
Monocyte	18	-0.01	0.19	0.62	0.53	0.52	0.79	0.67	0.57	0.31	0.34	0.60	0.37
Neutrophil	18	-0.53	-0.52	0.78	-0.21	-0.48	0.94	0.72	0.27	0.78	0.70	0.28	0.91
PBMC	n												
Monocyte	44	-0.45	-0.48	0.65	0.25	0.38	0.15	0.73	0.15	0.02	0.34	0.52	0.18

E PBMC

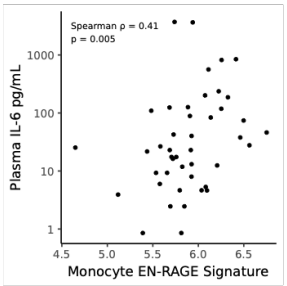

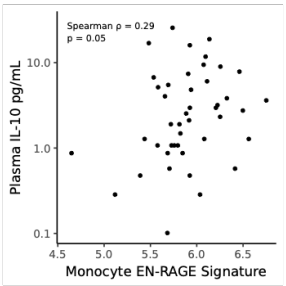

F ETA

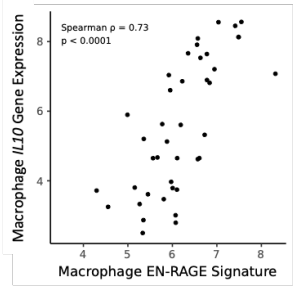

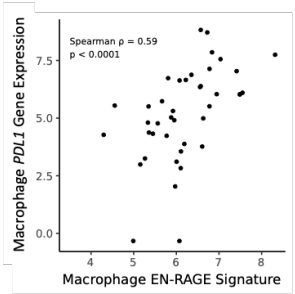

Figure 4. Characterization of myeloid and T cell immunosuppression phenotypes (COMET PBMC cohort).

A. EN-RAGE gene set score is most highly expressed in classical monocytes (cM) in PBMC CITE-seq data. ncM=non-classical monocytes, progen=progenitor cells. Cells were defined by marker genes as previously described(37). B. CD14, CD16, and HLA-DR surface protein expression across cell lineages in PBMC CITE-seq data. C-E. Spearman correlations between EN-RAGE gene set expression in classical monocytes and protein expression on C. classical monocytes, D. $CD4^+$ T cells and E. $CD8^+$ cells; n=128 samples, including 11 healthy controls. FDR<0.05 for all correlations, panel of 188 proteins measured. F-L Pseudobulked surface protein expression in 128 PBMC samples from 60 patients over 14 days in patients grouped by clinical outcomes. Classical monocyte expression of F. EN-RAGE gene signature, G. HLA-DR protein, H. PD-L1 protein. $CD8^+$ T cell expression of I. PD-1 and J. LAG3. $CD4^+$ T cell expression of K. PD-1 and L. LAG3. Blue line denotes the linear regression trend for gene expression over time. Red line denotes expression level in healthy controls. Vent. duration = days of mechanical ventilation in survivors. n=128 samples from 60 patients (429, 505 cells). Pearson correlation coefficients (r) and p values are indicated.

930

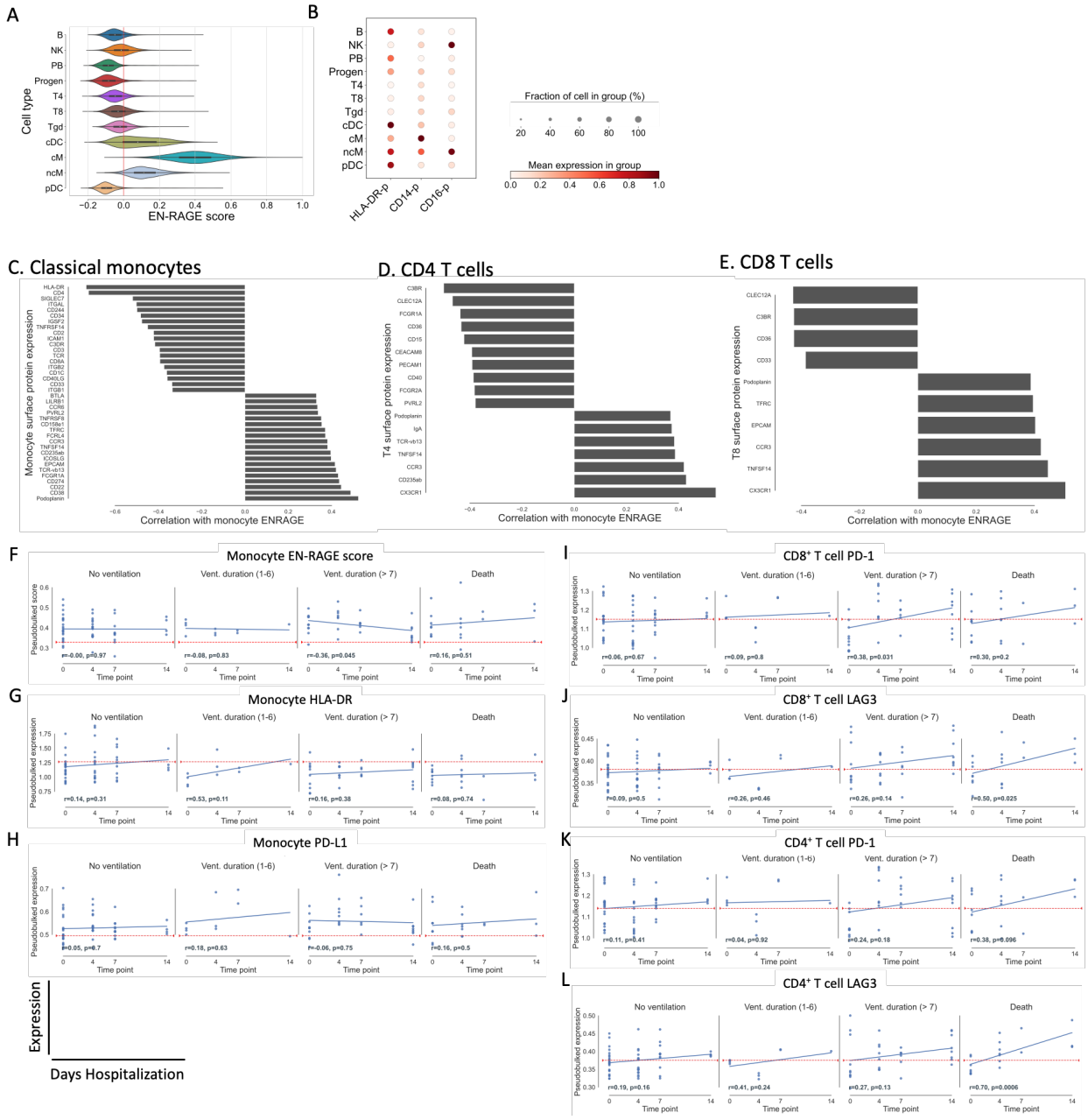
A
Cell type
B
NK
PB
Progen
T4
T8
Tgd
cDC
cM
ncM
pDC
EN-RAGE score
B
HLA-DR-p
CD14-p
CD16-p
Fraction of cell in group (%)
Mean expression in group
C. Classical monocytes
Monocyte surface protein expression
Correlation with monocyte ENRAGE
D. CD4 T cells
T4 surface protein expression
Correlation with monocyte ENRAGE
E. CD8 T cells
T8 surface protein expression
Correlation with monocyte ENRAGE
F
Monocyte EN-RAGE score
G
Monocyte HLA-DR
H
Monocyte PD-L1
I
CD8+ T cell PD-1
J
CD8+ T cell LAG3
K
CD4+ T cell PD-1
L
CD4+ T cell LAG3
No ventilation
Vent. duration (1-6)
Vent. duration (> 7)
Death
Pseudobulked score
Pseudobulked expression
Time point
Expression
Days Hospitalization

931

932

Figure 5. ENRAGE gene set enrichment analysis of monocytes treated with IL-6 *in vitro*. Monocytes stimulated with IL-6 for 24 hours compared with media, selected genes visualized as a heatmap using unsupervised clustering. A. ENRAGE signature genes. B. Genes associated with potential T cell suppressive functionality, from Supplemental Table 2. C. FGSEA analysis of EN-RAGE and MS1 signatures in IL-6 treated monocytes. Bars represent the normalized enrichment scores of how much each gene set is regulated by IL-6 treatment (BH adjusted p-value for MS1 < 0.01 and EN-RAGE < 0.001).

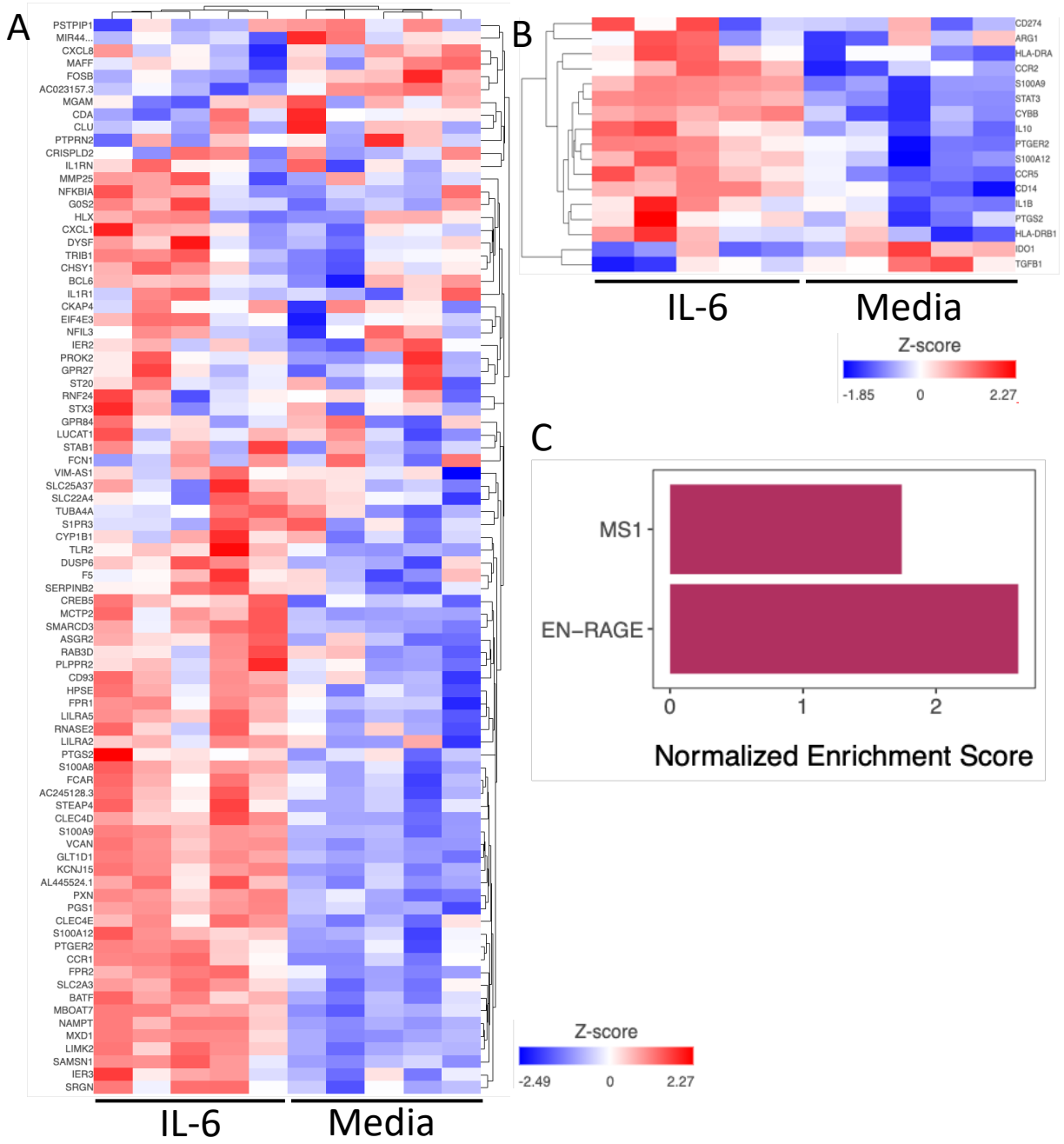

Figure 6. Severity-associated EN-RAGE gene set is associated with poor outcome and decreased by IL-6 blockade in COVID-19 patients (COVACTA cohort). **A.** Heatmap of EN-RAGE gene set associations with NIH ordinal scale severity at D1 (Severity NIH), need for new mechanical ventilation in patients not ventilated on D1 (Mech Vent), 28 day mortality (Death), treatment with tocilizumab or placebo at D3 or D7 relative to D1, and tocilizumab (TCZ) vs placebo at D7 relative to D1. **B-E.** Gene set enrichment analyses (GSEA) for gene sets associated with the myeloid cell states EN-RAGE, MS1(10), and MDSC(67) and T cells (CIBERSORT(45)). Normalized enrichment scores are shown, with red shading for t test $p<0.05$ and grey for $p>0.05$. TCZ = tocilizumab. For C and D, analyses were adjusted for baseline severity by incorporating baseline ordinal score as a covariate in our model. **F-G.** Tocilizumab treatment normalizes (F) EN-RAGE and (G) $CD8^+$ T cell gene expression to healthy levels more rapidly than placebo in survivors. Only patients with measurements for all three time points are included. Lines represent the mean expression value for the gene set signature score across tocilizumab- or placebo-treated subjects. Error bars represent the 95% confidence interval around the mean. Patients are split into those that were discharged before 28, those that remained hospitalized, or subjects that died by day 28. Average signature scores are shown across the first 7 days of treatment. CTRL=healthy controls, SOC = standard of care drug therapy; significance testing was performed using t-test comparing each day to D1 by study arm * = $p < 0.05$, ** = $p < 0.01$, *** = $p < 0.001$, **** = $p < 0.0001$.

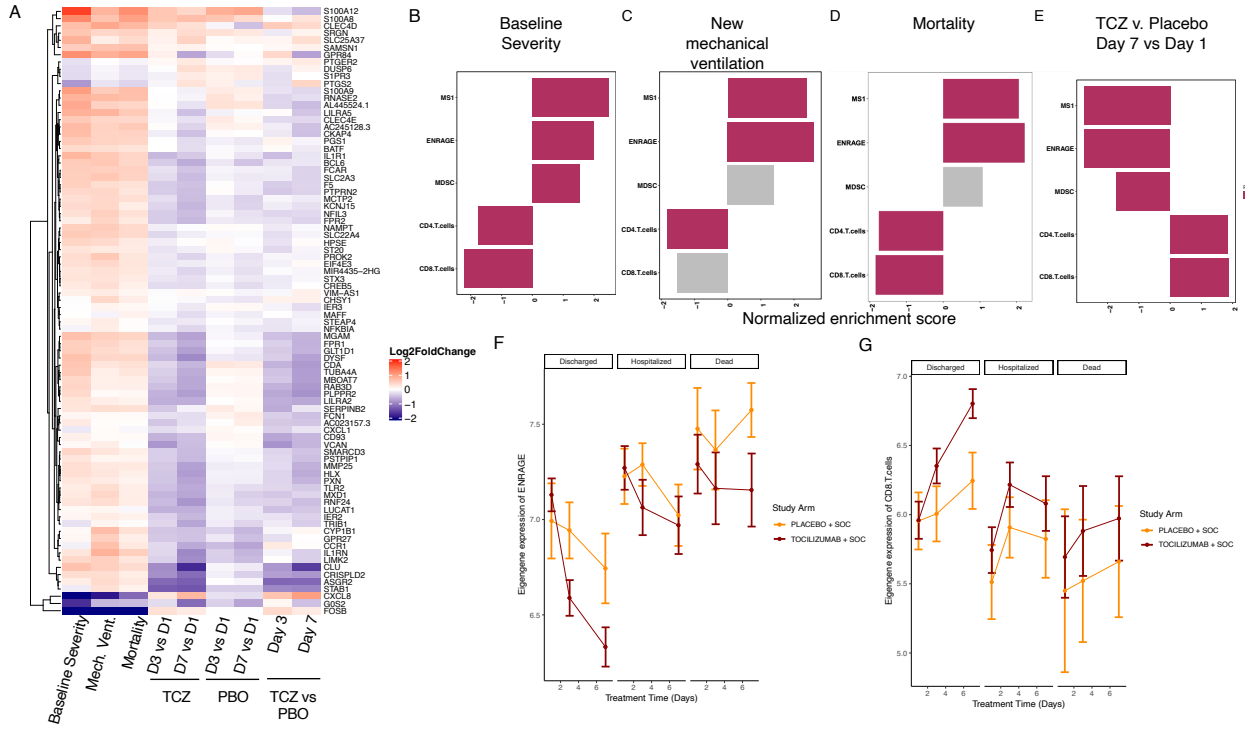
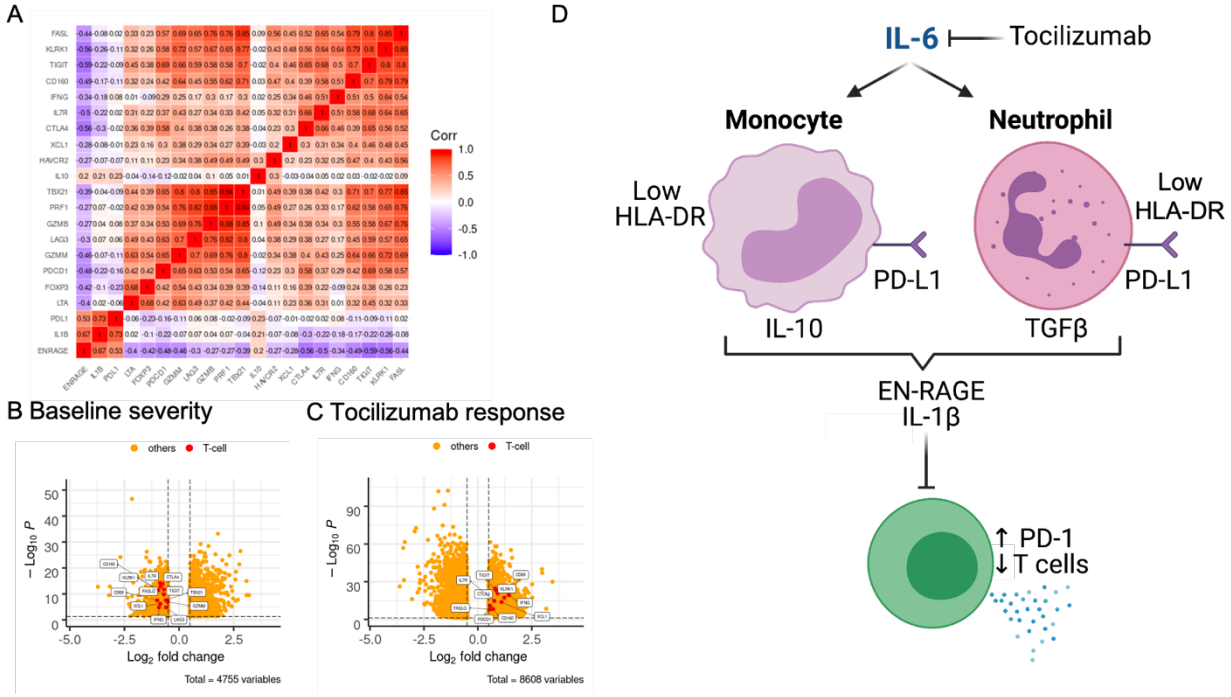
Figure 7. IL-6 blockade reduces potential T cell suppressive factors and normalizes T cells in COVID-19 patients (COVACTA cohort). A. EN-RAGE is positively correlated with IL-6-induced suppressive myeloid genes (*IL-10, IL-1b, PD-L1*) and inversely correlated with T cell genes (*FASL, LKRK1, TIGIT, CD160, IFNG, IL7R, CTLA4, XCL1, HAVCR2, TBX21, PRF1, GZMB, LAG3, GZMM, PDCD1, FOXP3*). Spearman correlation coefficients are shown for bulk whole blood gene expression. B-C. Volcano plots of reduced expression of T cell genes in A in patients with greater baseline severity (requiring positive pressure ventilation) versus not (B) and increased expression of T cell genes following 7 days treatment with tocilizumab (C). Dotted lines indicate absolute > 0.5 $\log_2$ fold change and FDR<0.05. D. Working model.